

UCSF

UC San Francisco Previously Published Works

Title

TCR signaling promotes formation of an STS1-Cbl-b complex with pH-sensitive phosphatase activity that suppresses T cell function in acidic environments

Permalink

<https://escholarship.org/uc/item/91f9m1qx>

Journal

Immunity, 56(12)

ISSN

1074-7613

Authors

Tsai, Yuan-Li
Arias-Badia, Marcel
Kadlecek, Theresa A
[et al.](#)

Publication Date

2023-12-01

DOI

10.1016/j.immuni.2023.11.010

Peer reviewed



HHS Public Access

Author manuscript

Immunity. Author manuscript; available in PMC 2024 December 12.

Published in final edited form as:

Immunity. 2023 December 12; 56(12): 2682–2698.e9. doi:10.1016/j.immuni.2023.11.010.

TCR signaling promotes formation of a STS1-Cbl-b complex with pH-sensitive phosphatase activity that suppresses T cell function in acidic environments

Yuan-Li Tsai¹, Marcel Arias-Badia², Theresa Kadlec¹, Yee May Lwin², Aahir Srinath², Neel H. Shah³, Zhi-En Wang⁴, Diane Barber⁵, John Kuriyan⁶, Lawrence Fong^{2,7}, Arthur Weiss^{1,8}

¹Rosalind Russell and Ephraim P. Engleman Rheumatology Research Center, Division of Rheumatology, Department of Medicine, University of California, San Francisco, CA 94143, USA

²Division of Hematology and Oncology, Department of Medicine, University of California, San Francisco, San Francisco, CA 94143, USA

³Department of Chemistry, Columbia University, New York, NY 10027, USA.

⁴Howard Hughes Medical Institute, University of California, San Francisco, San Francisco, CA 94143, USA

⁵Department of Cell and Tissue Biology, University of California, San Francisco, San Francisco, CA 94143, USA

⁶Department of Biochemistry, Vanderbilt University, Nashville, TN 37232, USA

⁷Helen Diller Family Comprehensive Cancer Center, University of California, San Francisco, San Francisco, CA 94143, USA

⁸Lead Contact

SUMMARY

T cell responses are inhibited by acidic environments. T-cell receptor (TCR)-induced protein phosphorylation is negatively regulated by dephosphorylation and/or ubiquitination but the

Corresponding Author: Arthur Weiss, MD, PhD, UCSF, Box 0795, 513 Parnassus, Room S-1032C, San Francisco, CA 94143-0795, phone: 415-476-8983, Arthur.Weiss@ucsf.edu.

AUTHOR CONTRIBUTIONS

Y.L.T. wrote the manuscript, planned and performed the research and analyzed and interpreted data. M.A.B. performed experiments and analyzed and interpreted data. T.K. performed experiments. N.S. analyzed data and reviewed the manuscript. Y.M.L. performed experiments. A.S. performed experiments. Z.E.W. performed experiments. D.B. advised experiments and reviewed manuscript. L.F. supervised and planned the research and reviewed the manuscript. J.K. supervised experiments. A.W. supervised and planned the research and edited the manuscript.

DECLARATION OF INTERESTS

A.W. is a co-founder and a scientific advisory board (SAB) member of Nurix Therapeutics, Inc., which has a Cbl-b inhibitor in phase I clinical trials. Dr. Weiss has founder shares and receives payment for his role on the Nurix SAB. A.W. also serves on advisory boards of BlueSphere Bio, BridGene Biologics, EpiBiologics, Genentech, Imidomics, and Jasper Therapeutics. L.F. has received research support from Roche/Genentech, Abbvie, Bavarian Nordic, Bristol Myers Squibb, Dendreon, Janssen, Merck, and Partner Therapeutics. L.F. has served on the SABs of Actym, Astra Zeneca, Atreca, Bioatla, Bolt, Bristol Myer Squibb, Daiichi Sankyo, Immunogenesis, Innovent, Merck, Merck KGA, Nutcracker, RAPT, Scribe, Senti, Sutro, and Roche/Genentech.

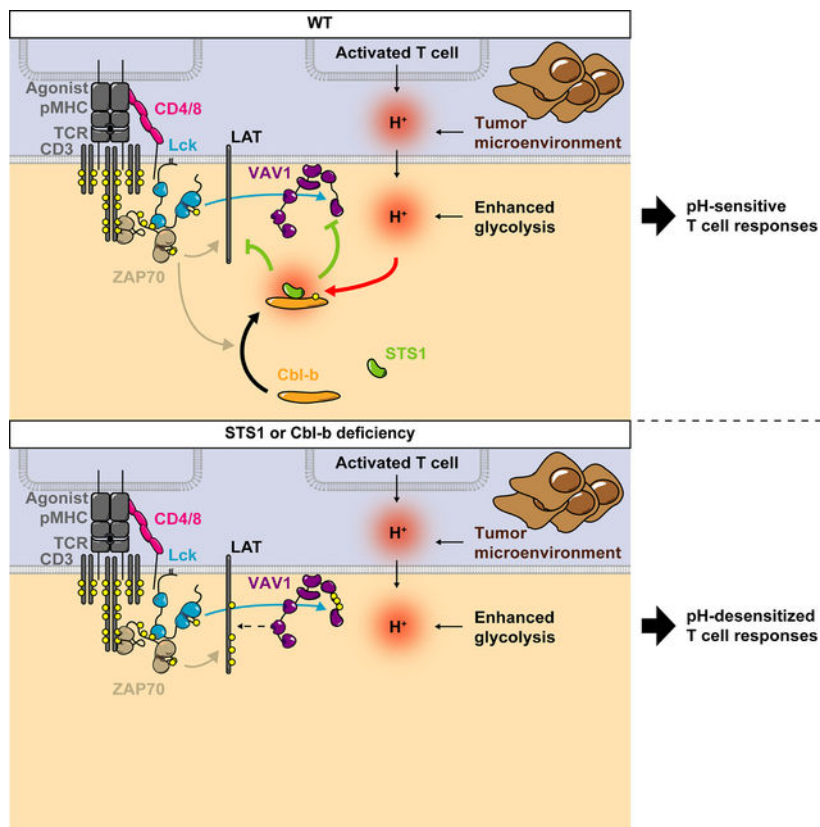
Publisher's Disclaimer: This is a PDF file of an unedited manuscript that has been accepted for publication. As a service to our customers we are providing this early version of the manuscript. The manuscript will undergo copyediting, typesetting, and review of the resulting proof before it is published in its final form. Please note that during the production process errors may be discovered which could affect the content, and all legal disclaimers that apply to the journal pertain.

mechanisms underlying sensitivity to acidic environments are not fully understood. Here, we found TCR stimulation induced a molecular complex of Cbl-b, an E3-ubiquitin ligase, with STS1, a pH-sensitive unconventional phosphatase. The induced interaction depended upon a proline motif in Cbl-b interacting with the STS1 SH3 domain. STS1 dephosphorylated Cbl-b interacting phosphoproteins. Deficiency of *STS1* or *Cbl-b* diminished sensitivity of T cell responses to the inhibitory effects of acid in an autocrine or paracrine manner *in vitro* or *in vivo*. Moreover, deficiency of *STS1* or *Cbl-b* promoted T cell proliferative and differentiation activities *in vivo*, and inhibited tumor growth, prolonged survival and improved T cell fitness in tumor models. Thus, a TCR-induced STS1-Cbl-b complex senses intra- or extra-cellular acidity and regulates T cell responses, presenting a potential therapeutic target for improving anti-tumor immunity.

eTOC blurb

T cell activities are suppressed in acidic pH conditions such as those found in tumor microenvironments. Tsai et al. reveal that a TCR-induced STS1-Cbl-b complex senses intra- or extra-cellular acidity and regulates T cell responses. STS1 or Cbl-b deficiency leads to acidic pH desensitization, improving anti-tumor reactivity and inhibiting tumor growth.

Graphical Abstract



Keywords

phosphatase; TCR signaling; pH sensing

INTRODUCTION

T cells are critically important for adaptive immunity. Therefore, maintaining their proper homeostasis and controlling the magnitude of their responses is critical to prevent immunopathology or auto-reactive responses to self-peptides bound to MHC molecules (self-pMHC). T cell receptor (TCR) signaling is mediated by regulated tyrosine phosphorylation initiated by the cytoplasmic tyrosine kinases Lck and ZAP70. Lck phosphorylates TCR immunoreceptor tyrosine-based activation motifs (ITAMs) in the ζ - and CD3-chains leading to the recruitment, phosphorylation, and activation of ZAP70¹. Activated ZAP70 phosphorylates downstream adaptor proteins including LAT and SLP76, which coordinate downstream signaling events^{2,3}. In the basal state, the TCR ITAMs are continuously phosphorylated as a consequence of TCR/self-pMHC interactions and some downstream signaling may ensue^{4,5}, but kinase substrates are dephosphorylated or ubiquitinated to maintain a basal homeostatic state⁶. A TCR-mediated response to an agonist pMHC requires a sufficiently long TCR-pMHC interaction to overcome a kinetic proofreading threshold allowing for the effects of downstream tyrosine phosphorylation pathways. Tyrosine phosphorylation of the ZAP70 activation loop as well as downstream events leading to phosphorylation of Y136 on LAT are necessary for PLC γ 1 recruitment, phosphorylation and activation^{7,8,9,10}. TCR induced phosphorylation events are negatively regulated by inhibitory receptors such as PD1, tyrosine phosphatases (PTPs), and E3 ligases such as Cbl-b and Grail^{11,12,13}. PD1 recruits the PTP SHP-2, which is implicated in negatively regulating TCR and CD28 signaling^{14,15}, emphasizing the importance of phosphorylation for effective T cell responses.

T cells constantly sense and respond to their local environments. Extracellular pH (pH_e) plays a critical role in regulating T cell function, as exemplified by VISTA which preferentially binds to PSGL-1 at acidic pH_e to suppress T cell function¹⁶. Acidification of intracellular pH (pH_i) is critical for limiting T cell responses. Deletion of the anion exchanger 2 (AE2), a major cell surface acid loader that reduces pH_i by extruding HCO_3^- in exchange for Cl^- , led to elevated pH_i , enhanced $\text{IFN}\gamma$ production, CD25 expression and proliferation in CD8^+ T cells^{17,18}. Interestingly, aged $\text{AE2}^{-/-}$ animals developed autoimmune cholangitis with intrahepatic accumulation of cytotoxic CD8^+ T cells and decreased expression of PD1¹⁹, thereby connecting the important role of acidic pH_i with suppression of T cell responses.

Multiple sources generate changes in pH_i and pH_e , including activities of plasma membrane HCO_3^- and H^+ transporters, V-ATPases as well as lactic acid resulting from increased T cell glucose metabolism during initiation of T cell responses leading to the acidification of pH_i ²⁰. Secreted lactic acid decreases the pH_e of lymph nodes (LNs) as an auto-regulatory mechanism to suppress T cell responses¹⁷, which may serve as negative feedback to limit immunopathology. Acidic pH_e has been reported to impair proliferation, CD25 and cytokine expression including $\text{IFN}\gamma$, $\text{TNF}\alpha$ and IL-2 as well as suppression of cytotoxic responses^{17,21,22,23}. Additionally, pH_e is decreased in the tumor microenvironment (TME) due to lactate secreted by tumor cells and relatively hypoxic conditions²⁴. Acidic pH_e also increases expression of immune checkpoints such as PD1, TIM3 and LAG3²⁵. Although

acidic pH_e has a negative effect on events downstream of the TCR, it is unclear how acidic pH_e is detected by T cells and influences TCR signaling.

Intriguingly, deletion of *Cbl-b* increases T cell infiltration and tumor rejection^{26,27}. Thus Cbl-b may play a role in overcoming acidic pH_e -induced immunosuppression. Casitas B-lineage Lymphoma (Cbl) proteins are E3 ligases involved in modulating TCR signaling. The Cbl protein family contains 3 members: c-Cbl, Cbl-b and the more distantly related Cbl-c²⁸. c-Cbl and Cbl-b are highly homologous but play different roles in T cells. *c-Cbl*^{-/-} mice exhibit altered positive selection during thymic development^{29,30}, whereas *Cbl-b*^{-/-} mice exhibit alterations in peripheral T cell activation^{31,32}. When TCR signaling is activated, Cbl forms complexes with multiple signaling molecules and ubiquitinates proteins leading to their degradation and consequent suppression of signaling events³³. In thymocytes, c-Cbl partners with the SRC-like adaptor protein to ubiquitinate the ζ -chain and causes the internalization of cell surface TCR³⁴, whereas in mature T cells internalization is mediated by Cbl-b³⁵. Interestingly, an *in vitro* kinetic study revealed that over 70% E3 ligase encounters with substrates are unproductive due to faster substrate dissociation than ubiquitination rates³⁶. Therefore, it is unclear how Cbl-b down-regulates the levels of phosphorylated proteins but has no effect on their total amounts during acute TCR stimulation, as seen in gain-of-function and loss-of-function studies^{37,38,39}. Instead, this discrepancy suggests the possible involvement of PTPs in modulating TCR signaling in a Cbl-b-dependent manner.

Suppressor of T-cell receptor signaling (STS) proteins are cytoplasmic PTPs modulating TCR signaling and consist of two members: STS1 and STS2. Both contain an N-terminal UBA domain, a Src homology 3 (SH3) domain and a C-terminal phosphatase domain⁴⁰. *In vitro*, STS1 has greater phosphatase activity than STS2⁴¹. STS1 and STS2 are recruited to the EGFR upon ligand stimulation and suppress receptor endocytosis in CHO cells⁴². In T cells, *STS1/2* double deficiency leads to accumulation of phosphorylated and ubiquitinated substrates, including ZAP70, following TCR stimulation^{43,44}. The loss of *STS1/2* exacerbates experimental autoimmune encephalomyelitis in animals, similar to *Cbl-b* deficiency⁴³. *STS1/2*^{-/-} (also referred to as *UBASH3B*^{-/-}/*3A*^{-/-}) mice were also found to exhibit enhanced protection against bacterial, fungal and viral infections⁴⁵⁻⁴⁷. In T cells, STS1 and STS2 are c-Cbl and Cbl-b binding partners⁴⁸. Whereas conventional PTPs use cysteine to catalyze dephosphorylation⁴⁹, STS1 and STS2 are exceptions because they use histidine as their catalytic residue⁵⁰. Interestingly, acidity increases STS1 affinity to the model substrate *p*-nitrophenylphosphate, enhancing its catalytic rate in acidic pH ⁴¹.

We set out to determine whether Cbl proteins or STS phosphatases might play a role in sensitizing T cells to acidic pH . Upon TCR stimulation, Cbl-b served as an adaptor to recruit STS1. In TCR-stimulated Jurkat leukemic T cells, recruited STS1 dephosphorylated Cbl-b-bound substrates. Primary mouse T cells deficient in either *STS1* or *Cbl-b* alone or both exhibited hyperresponsiveness and resistance to acidic pH_e -induced T cell suppression. Moreover, mice deficient in either *STS1* or *Cbl-b* had improved responses to antigen, delayed tumor growth and improved survival and T cell fitness.

RESULTS

TCR stimulation induces Cbl-b and STS1 to interact and regulate the TCR signaling pathway

Using CRISPR/Cas9, we deleted *c-Cbl* or *Cbl-b* in Jurkat cells and depleted the remaining Cbl-b or c-Cbl proteins using siRNA, respectively. Deletion of *c-Cbl* or *Cbl-b* enhanced tyrosine phosphorylation of many TCR signaling proteins including PLC γ 1, VAV1, ZAP70 and LAT, with a further increase in doubly depleted cells under both unstimulated and TCR-stimulated conditions. Interestingly, total protein amounts of the phosphoproteins remained unchanged (Fig. 1A and Table S1), even out to 6 hours (Fig. S1A and Table S2). These results are consistent with earlier studies suggesting Cbl proteins down-regulate phosphorylated proteins without degrading them^{37,38}, and implicate the potential involvement of a Cbl-associated tyrosine phosphatase in regulating basal and stimulated phosphorylation of these proteins.

The phosphatases STS1 and STS2 were identified as c-Cbl and Cbl-b binding partners in a large-scale proteomic study⁴⁸. We identified a TCR-inducible and preferential interaction between STS1 and Cbl-b in Jurkat cells (Fig. 1B), and confirmed this in primary mouse T cells (Fig. S1B). Next, we deleted *STS1* in WT and *Cbl-b*^{-/-} Jurkat cells, and found that *STS1* deletion resulted in elevated basal and stimulated TCR signaling, nearly phenocopying *Cbl-b*^{-/-} cells. The doubly deficient cells had levels of phosphoproteins similar to those in the singly deficient cells (Fig. S1C and Table S3). These results suggest STS1 plays a major role in regulating basal and TCR-inducible protein phosphorylation.

To define the basis of the Cbl-b-STS1 interaction, we created truncation mutants of Cbl-b (Fig. S1D), and found STS1 binds to Cbl-b between residues 430 to 529 (Fig. S1E). This segment contains several proline-rich regions (PRRs) (Fig. S1D), and we suspected STS1 binds to one of these PRRs using its SH3 domain. Indeed, the STS1 SH3 domain-defective mutant W295A lost its interaction with Cbl-b (Fig. 1C–D). Three PRRs in Cbl-b located between residues 430 to 529 were individually mutated (Fig. 1E)⁵¹. Mutating the PPVPP motif resulted in the loss of interaction with STS1 (Fig. 1F). Using Far-Western blotting, we determined the STS1 SH3 domain could bind the Cbl-b PPVPP motif directly (Fig. S1F). The PPVPP motif is highly conserved in 26 mammals (Fig. S1G), suggesting this motif has functional importance.

We reconstituted *STS1*^{-/-} Jurkat cells with the WT or mutants defective in ubiquitin-associated (M47A), SH3 (W295A) or phosphatase domains (H391A), and *Cbl-b*^{-/-} Jurkat cells with WT or the PPVPP mutant (AAVAA), respectively. Both WT and M47A suppressed phosphorylation of TCR signaling molecules following stimulation, but not the W295A and H391A mutants (Fig. S2A). In agreement, both W295A and H391A were less able to suppress TCR-induced phospho-Erk and CD69 (Fig. S2B–C). Similarly, the AAVAA Cbl-b mutant exhibited partially reduced suppressive activity for TCR-induced phosphoproteins (Fig. S2D), and failed to substantially suppress phospho-Erk and CD69 induction (Fig. S2E–F). Together, these results demonstrate that STS1 and Cbl-b are both potent suppressors of TCR signaling and their interaction is critical for their suppressive activities.

Phosphorylation of Cbl-b Y363 triggers a major conformational change to expose the RING domain⁵², suggesting phosphorylation of Cbl-b might be involved in accessing the PRRs. Treating the cells with either the Src family kinase (SFK) inhibitor PP2 or using *ZAP70*^{-/-} Jurkat cells impaired the Cbl-b-STS1 interaction (Fig. S3A–B). Treating the PP1 analog-sensitive mutant *ZAP70*-expressing P116 cells, which are sensitive to the mutant-specific inhibitor 3-MB-PP1⁵³, with either PP2 or 3-MB-PP1 inhibited the Cbl-b-STS1 interaction (Fig. S3C). Since *ZAP70* is downstream of SFKs, these results suggested that *ZAP70* may play a more direct role in inducing Cbl-b-STS1 interaction. Early studies revealed that CD3 stimulation leads to an interaction between *ZAP70* and Cbl-b as well as to Cbl-b phosphorylation⁵⁴, suggesting that phosphorylation of Cbl-b by *ZAP70* might induce the binding of STS1 to Cbl-b.

To determine which Cbl-b domains are involved in the recruitment of STS1, we reconstituted *Cbl-b*^{-/-} Jurkat cells with Cbl-b defective mutants in the *ZAP70*-binding (G298E), ligase-activating phosphorylation site (Y363F), E3 ligase (C373A), putative phosphorylation sites/SH2 domain-binding (3YF: Y665F, Y709F and Y889F), and UBA domain (M940A) (Fig. S3D). As shown in Fig. S3E, the G298E mutant failed to inducibly recruit STS1, as did 3YF and M940A mutants, with the latter reported to suppress Cbl-b phosphorylation⁵⁵. The requirement of *ZAP70* catalytic activity, together with G298E and 3YF mutant effects, strongly suggested that *ZAP70* might phosphorylate Y665, Y709 and/or Y889. On the other hand, neither the C373A nor Y363F mutations prevented STS1 recruitment (Fig. S3E). *ZAP70* favors substrates surrounded by acidic residues, particularly at the -1 position⁵⁶, which are present in Y665, Y709 and Y889 of Cbl-b (Fig. S3F). Therefore, we reconstituted *Cbl-b*^{-/-} Jurkat cells with single, double, or triple non-phosphorylatable mutants at these residues. All mutants containing Y709F failed to inducibly recruit STS1 (Fig. S3G). We further reviewed data from a high-throughput kinase specificity assay in which Lck and *ZAP70* were previously characterized⁵⁷. As shown in Fig. S3H, peptides corresponding to known substrates of Lck, ζ Y123 and Y142, were favorably phosphorylated by Lck but not *ZAP70*, whereas known substrates of *ZAP70*, LAT Y171 and Y226, were favorably phosphorylated by *ZAP70* but not by Lck. For Cbl-b, while Y665 and Y889 were both good substrates for Lck and *ZAP70*, Y709 was a poor substrate for Lck but highly favored by *ZAP70*. These results were consistent with our observation that *ZAP70* kinase activity is essential for the inducible Cbl-b-STS1 interaction (Fig. S3C). Sequence conservation analysis indicated that Y709 and surrounding residues are highly conserved in mammals (Fig. S3I), suggesting its functional importance. Furthermore, Cbl-b Y709F suppressive activity was diminished, as shown by higher phosphorylation as well as phospho-Erk and CD69 induction (Fig. S3J–L). Thus, phosphorylation of Cbl-b Y709 by *ZAP70* drives the TCR inducible recruitment of STS1 to Cbl-b and is critical for Cbl-b suppressive activity.

We detected increased phosphorylated signaling molecules, including LAT and VAV1, bound to Cbl-b following TCR stimulation of *STS1*^{-/-} cells (Fig. 1G and Table S4). Furthermore, cells expressing WT STS1 or the UBA domain-defective mutant M47A exhibited reduced phosphorylated substrates bound to Cbl-b, but not in cells reconstituted with the SH3 (W295A) or phosphatase-defective (H391A) STS1 mutants (Fig. 1H and Table S5). Likewise, *Cbl-b*^{-/-} cells reconstituted with WT Cbl-b exhibited markedly decreased

phosphoproteins bound to the transduced Cbl-b, but not the STS1 binding-defective mutant AAVAA (Fig. 1I and Table S6). Together, these results suggest that STS1 is inducibly recruited to Cbl-b where it dephosphorylates phosphoproteins bound to Cbl-b following TCR stimulation.

Cbl-b and/or STS1 deficiency leads to CD28 co-stimulation independence

STS1^{-/-}, *Cbl-b*^{-/-} and *STS1*^{-/-}/*Cbl-b*^{-/-} mice had no obvious phenotypic effects on thymic development (Fig. S4A). A reduced CD4/CD8 ratio was observed in mature *STS1*^{-/-} and *Cbl-b*^{-/-} T cells and even more in the *STS1*^{-/-}/*Cbl-b*^{-/-} cells (Fig. S4B). The 6–8-week old *STS1*^{-/-}/*Cbl-b*^{-/-} mice exhibited higher effector memory (EM) populations (CD44⁺ CD62L⁻) in CD4⁺ T cells, and higher central memory (CM) population (CD44⁺ CD62L⁺) in both CD4⁺ and CD8⁺ T cells, while naive populations (CD44⁻ CD62L⁺) were lower in both CD4⁺ and CD8⁺ T cells. For singly deficient animals, *STS1* deficiency led to increased CM and lowered naive CD8⁺ T cells, whereas *Cbl-b* deficiency resulted in increased CM in CD8⁺ and reduced naive subsets in both CD4⁺ and CD8⁺ T cells (Fig. S4C–D). In addition, no clear defects in the thymus-derived or peripheral regulatory (CD25⁺ FoxP3⁺) T cells, nor in the anergic (CD73⁺ FR4⁺) T cells in CD44⁺ and CD44⁻ populations were observed in singly or doubly deficient mice (Fig. S4E–F).

It has been reported that the loss of *Cbl-b* results in IL-2 production in a CD28-independent manner in response to T cell stimulation^{32,35}. Interestingly, CD3 stimulation alone was sufficient to induce IL-2 secretion in *STS1*^{-/-} T cells at a comparable level to the *Cbl-b*^{-/-} T cells, but double deficiency did not further enhance the response (Fig. S4G). CD3/CD28 co-stimulation led to robust IL-2 production in the WT as well as *STS1*^{-/-} and *Cbl-b*^{-/-} T cells, which was not further substantially enhanced in *STS1*^{-/-}/*Cbl-b*^{-/-} cells, suggesting T cells deficient in *STS1* or *Cbl-b* became at least partially independent of CD28 co-stimulation.

Sensitivity of T cell responses to acidic pH_e depends upon Cbl-b or STS1

STS1 catalytic rate has been previously reported to be sensitive to acidic pH⁴¹, which we confirmed in an *in vitro* phosphatase assay (Fig. 2A). We observed a 3.8-fold increase in catalytic rate when pH was reduced from 7.5 to 6.5 which further increased at lower pH. This was contrasted by SHP1, a conventional cytoplasmic PTP expressed in T cells, which showed maximal catalytic rate at pH 7 (Fig. 2A). Consistent with a previous report, STS2 possessed markedly reduced activity⁵⁸ (Fig. 2A). STS1 binding to Cbl-b was independent of acidic pH_e (Fig. 2B). To determine the effect of the pH_e on the pH_i of T cells, primary WT mouse T cells were loaded with the pH-sensitive fluorescent dye BCECF. The dye is membrane-permeable but once its methyl ester moiety is cleaved by intracellular esterases, it is trapped within the cells⁵⁹. At pH_e above 6.8, T cells maintained a relatively neutral pH_i. However, at pH_e below 6.8, although T cells could partially elevate pH_i, the acidic pH_e still caused a reduction of pH_i (Fig. 2C), suggesting STS1 in the T cell cytoplasm is sensitive to more profound ranges of acidic pH_e.

Numerous studies have indicated that acidic pH_e impairs T cell function (reviewed in⁶⁰). We stimulated CD4⁺ and CD8⁺ T cells *in vitro* in medium adjusted to a starting pH_e 7.4 or 6.6. Sub-optimal stimulation was used with our expectation that deletion of *Cbl-b* or *STS1*

would elevate T cell responses^{61,62}. As shown in Fig. 2D and S5A, acidic pH_e significantly suppressed WT CD8⁺ T cell proliferation but not *STSI*^{-/-} or *Cbl-b*^{-/-} T cells. *STSI*^{-/-}/*Cbl-b*^{-/-} T cells responded similarly to the singly deficient cells. Likewise, up-regulation of CD25 (Fig. 2E and S5B), granzyme B (Fig. 2F and S5C) and IFN γ production (Fig. 2G) were significantly inhibited by acidic pH_e in WT cells, but not in singly or doubly deficient T cells. Similarly, WT CD4⁺ T cell proliferation, CD25 and IL-2 production as well as CD44 expression both in CD4⁺ and CD8⁺ WT cells were potently inhibited by acidic pH_e , but not in any of the deficient cells (Fig. S5D–H). Together, these results indicate that the suppression of T cell function by acidic pH_e is at least partially due to enhanced activity of STS1. Since STS1 function relies on Cbl-b binding, the loss of Cbl-b phenocopies the loss of STS1. Because double deficiency did not further enhance the responses, we only utilized singly deficient animals and cells in the subsequent experiments.

Sensitivity of T cell responses to acidic pH_e depends up on the Cbl-b-STS1 interaction and the histidine-containing phosphatase domain of STS1

To investigate the roles of STS1 and Cbl-b in mediating low pH_e induced T cell suppression under more physiological conditions, we stimulated OT-1 T cells with a peptide fragment of chicken ovalbumin (OVA_{257–264}) and a series of weaker peptide agonists derived from OVA and measured the induction of CD69. As shown in Fig. S6A, under physiologic pH_e , high affinity agonists OVA and Q4R7 peptide⁶³ strongly induced CD69 expression in WT, *STSI*^{-/-} or *Cbl-b*^{-/-} T cells. The weaker stimuli Q4H7 and G4 showed differences in responses, where *Cbl-b*^{-/-} T cells exhibited the strongest CD69 induction, followed by *STSI*^{-/-} and then WT T cells. However, acidic pH_e reduced the sensitivity of WT cells to OVA and weaker peptides Q4H7 and G4 (Fig. 3A). In contrast, CD69 was up-regulated in *STSI*^{-/-} or *Cbl-b*^{-/-} T cells in a pH-insensitive manner. Similarly, long-term stimulation with OVA peptides at acidic pH_e lowered the proliferative response of WT cells but not *STSI*^{-/-} or *Cbl-b*^{-/-} T cells (Fig. S6B), indicating acidic pH_e , STS1, and Cbl-b regulate T cell signaling by altering the activation threshold.

To determine how STS1 contributes to suppress TCR responses by acidic pH_e , we utilized murine STS1 mutants that were defective in the SH3 (W284A) or phosphatase domain (H380A). We also replaced the STS1 phosphatase domain with that of the SHP1 phosphatase (Fig. 3B), which showed optimal catalytic rate at pH 7 and did not vary greatly with pH (Fig. 2A). We demonstrated that the STS1-SHP1 chimera was functionally sufficient to attenuate CD69 expression stimulated by G4 peptide stimulation (Fig. 3C). As shown in Fig. 3D–E, following stimulation by G4 peptide, CD69 induction was suppressed in *STSI*^{-/-} cells reconstituted with WT STS1 under acidic conditions. However, the acidic pH_e failed to suppress CD69 up-regulation in *STSI*^{-/-} cells expressing W284A or H380A mutants. In addition, *STSI*^{-/-} T cells reconstituted with pH_e-insensitive STS1-SHP1 chimera, with or without a defective STS1 SH3 domain, were able to induce CD69 in acidic pH_e at a similar level as those in physiologic pH_e . These results suggest that the STS1 phosphatase domain is responsible for mediating the acidic pH_e -induced inhibition of the TCR-mediated response. These results also emphasize the importance of a functional SH3 domain of STS1.

To test the role of STS1 recruitment in Cbl-b-mediated pH_e sensitivity in T cells, we utilized an STS1 binding-defective mutant AAVAA. For comparison, an E3 ligase defective mutant C373A, which has been shown to confer hyperactivity to TCR responses⁶⁴, was included (Fig. 3F). Because the reconstituted T cells expressed high basal CD69, we measured IFN γ expression in the transduced cells in response to G4 peptide under different pH_e conditions. As shown in Fig. 3G, in WT Cbl-b reconstituted T cells, IFN γ expression was significantly suppressed in acidic pH_e, whereas IFN γ expression in AAVAA-reconstituted cells was insensitive to acidic pH_e. Interestingly, acidic pH_e also suppressed IFN γ expression in C373A-reconstituted cells, indicating Cbl-b-mediated acidic pH_e-induced T cell suppression depends on STS1 interaction but not E3 ligase activity.

Next we focused on identifying differences in STS1 and Cbl-b in suppressing TCR signaling. Early studies reported that Cbl proteins contribute to TCR internalization via ζ ubiquitination, mediated by their E3 ligase activities^{35,34}. As shown in Fig. S7, CD3 ligation led to down-regulated cell surface CD3 in WT and *STS1*^{-/-} cells, but not *Cbl-b*^{-/-} T cells. Together, these results demonstrated that the acidic pH_e-induced TCR suppression depends on the Cbl-b-STS1 interaction and the phosphatase domain of STS1. However, only Cbl-b possesses the additional ability to suppress TCR signaling by down-regulating the receptor.

Similar impact of *STS1* and *Cbl-b* deficiency on *in vivo* antigen-specific T cell responses

A recent study revealed that LNs maintain some acidic regions, the result of T cell induction of glycolytic metabolism that generates lactic acid¹⁷. To investigate the roles of STS1 and Cbl-b in limiting the response of T cells *in vivo*, we first examined antigen specific T cell proliferative responses to antigen in LNs. OT-1 T cells were labeled with CellTrace dyes. OT1 WT cells were mixed with OT1 *STS1*^{-/-} or OT1 *Cbl-b*^{-/-} cells and adoptively transferred into congenic hosts, followed by ovalbumin injection in one hind-limb footpad. In the draining popliteal LNs there was a higher percentage of *STS1*^{-/-} T cells that had divided and more cells were able to enter multiple proliferation cycles compared with the WT (Fig. 4A–C). Likewise, *Cbl-b*^{-/-} T cells also showed a higher proliferative response *in vivo* (Fig. 4D–F). However, there were no differences in CD44 and TCF1 expression between proliferated WT and *STS1*^{-/-} or *Cbl-b*^{-/-} cells (Fig. 4G–J). A significant difference in PD1 expression was only observed in *Cbl-b*^{-/-} cells (Fig. 4K–L). For CXCR3, a difference was only observed in *STS1*^{-/-} cells (Fig. 4M–N).

We examined T cell differentiation in the LNs. OT-2 T cells were adoptively transferred into congenic hosts, followed by subcutaneous ovalbumin injection at the right flank. In the draining inguinal LNs the populations of T follicular helper (Tfh) cells were significantly increased in *STS1*^{-/-} and, even more strongly in *Cbl-b*^{-/-} T cells, as shown by expanded PD1⁺ CXCR5⁺ population (Fig. 4O) and CXCR5⁺ Bcl-6⁺ population (Fig. 4P). Together, these results demonstrated that deletion of *STS1* or *Cbl-b* increased T cell proliferative and differentiation responses *in vivo*.

T cells are exposed to autocrine and paracrine acid sources

Upon activation, T cells up-regulate glycolysis which can result in release of lactic acid⁶⁵. The Na⁺/H⁺ antiporter (NHE1) is a ubiquitous cell surface transporter responsible for efflux

of intracellular H^+ ⁶⁶. To test whether T cells can sense the acid produced by themselves (an autocrine effect), we stimulated T cells in pH_e -neutral medium and treated them with EIPA, a specific and potent inhibitor for NHE1. As shown in Fig. 5A, EIPA treatment effectively reduced the pH_i of activated T cells. Similar to the effects of acidic pH_e (Fig. 2D–F), blocking H^+ secretion led to suppressed proliferation and reduced CD25 and granzyme B expression in WT but not *STSI*^{-/-} and *Cbl-b*^{-/-} cells (Fig. 5B), suggesting that the STS1/Cbl-b axis was sensitive to acid produced within T cells, perhaps reflecting a capacity of T cells to restrain their own activity as negative feedback regulation.

To investigate whether T cells can sense acid via a paracrine route *in vivo*, we first determined whether T cells secrete acid in the LNs during an immune response. We immunized OT-1 mice with ovalbumin in the footpad to induce maximal T cell activation (Fig. 5C). The cells within acidic pH_e were probed using a fluorophore-labeled pH-Low Insertion Peptide (pHLIP) that undergoes a conformational change and inserts into the membrane stably at low pH_e ^{67–69}. In both draining and contralateral LNs, even though the percentage is low in the contralateral LNs, activated (CD44^{Hi}) OT-1 T cells exhibited higher pHLIP MFI than the naive (CD44^{Lo}) subset (Fig. 5D–E), suggesting the activated T cells are the sources of acid that acidified the pH_e around themselves.

Using this model, we adoptively transferred Pmel-1 T cells into OT-1 mice followed by ovalbumin immunization and pHLIP labeling. Since Pmel-1 T cells do not respond to ovalbumin, they remained naive after the immunization (Fig. 5F). In the contralateral LNs, the pHLIP intensity of Pmel-1 T cells was similar to that of CD44^{Lo} OT-1 T cells. However, in the draining LNs where a large portion of OT-1 T cells were activated, a substantial subset of Pmel-1 T cells was enriched for higher pHLIP staining, suggesting they were exposed to acid secreted by the activated OT-1 cells, thereby providing evidence that paracrine production of acid by T cells can be detected *in vivo* (Fig. 5G). We will provide evidence below that STS1 and Cbl-b can impart sensitivity to acidic pH_e produced via a paracrine mechanism.

Enhanced anti-tumor activities in *STSI* and *Cbl-b* deficient animals or if TME acidic pH is reduced

The TME is generally acidic due to poor vascularization, rapid metabolism and glycolytic activities of tumor cells²⁴. The murine prostate adenocarcinoma TRAMP-C2 tumor model produces an acidic TME^{70,71,72}, and the tumor cells express an immunodominant antigen, Spas-1. T cell responses against tumor epitope can be identified using Spas-1 peptide-coupled MHC Class I tetramers²⁴. Using this model, we found that either *STSI*^{-/-} or *Cbl-b*^{-/-} mice exhibited diminished tumor growth (Fig. 6A–B), and prolonged survival (Fig. 6C). Although overall tumor-infiltrating CD8⁺ T cells were only significantly increased in *Cbl-b*^{-/-} mice (Fig. 6D), the Spas-1-reactive subsets in either *STSI*^{-/-} or *Cbl-b*^{-/-} CD8⁺ T cells were significantly expanded (Fig. 6E). Furthermore, *STSI*^{-/-} or *Cbl-b*^{-/-} tumor-reactive T cells expressed higher levels of TCF1 (Fig. 6F), a key transcription factor required for the formation of memory precursor CD8⁺ T cells and is lost in terminally exhausted T cells^{73–75}. Consistently, *STSI*^{-/-} or *Cbl-b*^{-/-} Spas-1-specific T cells showed decreased levels of exhaustion markers including PD1, TIM3 and LAG3 (Fig. 6G–H), as

well as a higher frequency of PD1⁻ TIM3⁻ LAG3⁻ population (Fig. 6H). The expression of the effector molecule perforin (PRF1) was increased in tumor-reactive *STSI*^{-/-} or *Cbl-b*^{-/-} T cells (Fig. 6I). Thus, both deficient mice have significantly improved T cell fitness in their anti-tumor responses. Spas-1-reactive CD8⁺ T cells were also detected at higher frequencies in the spleens of *STSI*^{-/-} or *Cbl-b*^{-/-} mice (Fig. 6J). When re-stimulated *ex vivo*, *STSI*^{-/-} or *Cbl-b*^{-/-} Spas-1-specific T cells up-regulated granzyme B in an acidic pH_e-insensitive manner, but WT cells did not (Fig. 6K).

In support, we applied B16-F10 melanoma model which also generates an acidic TME⁷⁶, using WT, *STSI*^{-/-} or *Cbl-b*^{-/-} mice expressing the Pmel-1 TCR transgene, reactive to the endogenous tumor-associated antigen glycoprotein 100 (gp100)⁷⁷. Consistent with the TRAMP-C2 model, loss of *STSI* and *Cbl-b* reduced the tumor burden (Fig. 7A) and improved survival (Fig. 7B). For tumor-infiltrating T cells, in *STSI*^{-/-} or *Cbl-b*^{-/-} increased infiltration and effector populations were observed (Fig. 7C–D). More importantly, *STSI*^{-/-} and *Cbl-b*^{-/-} cells demonstrated higher frequencies of PD1⁻ TIM3⁻ LAG3⁻ population (Fig. 7E–F) and lower frequencies of terminally exhausted T cells co-expressing PD1, TIM3 and LAG3 (Fig. 7G) as well as the transcription factor Tox (Fig. 7H), associated with terminal T cell exhaustion⁷⁸. Higher percentages of CD44⁺ CD62L⁻ effector Pmel-1 T cells were also found in the spleens of *STSI*^{-/-} and *Cbl-b*^{-/-} mice (Fig. 7I). When stimulated *ex vivo*, *STSI*^{-/-} and *Cbl-b*^{-/-} Pmel-1 T cells up-regulated CD69 in an acidic pH_e-insensitive manner (Fig. 7J). Finally, in an *in vitro* killing assay, we found that acidic pH_e impaired the cytolytic activity of *in vitro* generated WT cells but not the *STSI*^{-/-} or *Cbl-b*^{-/-} cytotoxic T cells (Fig. 7K). These findings demonstrate the pivotal contribution of STS1 and Cbl-b to tumor-mediated immunosuppression.

Cancer cells are known to maintain a higher pH_i as well as a lower pH_e⁷⁹, achieved by up-regulating the expression and/or activity of cell surface acid-extruders such as NHE1 and the proton pump H⁺-ATPase⁷⁹. Interestingly, it was reported that the acidity of the TME in the B16 melanoma is sensitive to the proton pump inhibitor (PPI) esomeprazole²¹. Treating mice with esomeprazole increased TME pH_e, proliferative potential and cytokine production of tumor-infiltrating T cells²¹.

Using the pHLIP peptide⁷⁸, we demonstrated that PPI treatment significantly reduced the acidity of TME in B16 melanoma model (Fig. 7L). PPI treatment reduced tumor burden of WT mice to a similar level seen in *STSI*^{-/-} and *Cbl-b*^{-/-} mice (Fig. 7M), and led to reduced levels of T cell exhaustion markers and decreased the PD1⁺ TIM3⁺ LAG3⁺ population in WT mice to comparable levels with *STSI*^{-/-} and *Cbl-b*^{-/-} cells (Fig. 7N–O). In addition, PPI enhanced WT cell proliferative activity and CD8⁺/T_{reg} (CD4⁺ FoxP3⁺) ratio (Fig. 7P–Q). Interestingly, PPI did not cause significant changes in *STSI*^{-/-} and *Cbl-b*^{-/-} cells, meaning the removal of *STSI* and *Cbl-b* desensitized T cells to suppressive pH_e acidity. Moreover, PPI did not have a statistically significant effect ($p = 0.1143$) on T cell pH_i directly (Fig. 7R), nor on T cell functions (Fig. 7S). Since *STSI*^{-/-} and *Cbl-b*^{-/-} cells were insensitive to pH_e manipulation, these results demonstrated that acidic pH_e, created via a paracrine pathway *in vivo*, significantly restrained T cell function via the STS1/Cbl-b axis.

DISCUSSION

To prevent unwanted responses to self-pMHC and to control the magnitude of responses to agonist pMHC, T cells' activities must be tightly regulated. Here, we identified a fundamental molecular mechanism responsible for attenuating T cell functions in acidic environments and made several observations that could have implications in regulating T cell activities in physiological immune responses and pathological conditions. We found critical roles for a TCR-inducible complex formed by Cbl-b with the unconventional PTP STS1 in mediating T cell sensitivity to acidic pH.

First, we demonstrated that STS1 is preferentially and inducibly recruited by Cbl-b following TCR stimulation. We identified the PRR in Cbl-b that STS1 binds to, and found that ZAP70 phosphorylation of Cbl-b Y709 is essential for the inducible interaction. How Cbl-b Y709 phosphorylation results in STS1 binding to the PRR is unclear. The C-terminus of Cbl-b is largely intrinsically disordered (ID). ID regions commonly participate in multivalent interactions, as they function as scaffolds^{80,81,82,83}. Interestingly, phosphorylation and other post-translational modifications (PTMs) are often preferentially enriched in the ID regions^{84,85}. Such PTMs have been shown to function as the allosteric modulators driving interactions at distal sites^{83,86}. Interestingly, the adaptor protein CrkL, reported to selectively bind to Cbl-b pY709⁸⁷, demonstrates strong co-recruitment correlation with STS1 binding to Cbl-b⁴⁸. This might suggest that CrkL binding to pY709 somehow allosterically exposes the PRR allowing STS1 binding.

We demonstrated the importance of STS1 recruitment to Cbl-b in regulating the TCR signaling. When the TCR is stimulated, Lck and ZAP70 are induced to phosphorylate downstream substrates. Some of the phosphorylated substrates can bind to Cbl-b through different functional domains³³. The simultaneous concentration of phosphorylated substrates and the recruitment of STS1 to Cbl-b enables STS1 to conveniently dephosphorylate Cbl-b-bound substrates. This was associated with suppression of downstream TCR signaling events. Although it contains a functional E3 ligase domain, the Cbl-b STS1-binding defective mutant indicated that the E3 ligase activity is not sufficient to rapidly down-regulate phosphorylated substrates. This is possibly due to high unproductive rate of ubiquitination as reported previously³⁶. Thus, recruiting STS1 is critically important to allow T cells to modulate the signaling magnitude rapidly and reversibly during early TCR stimulation. It is likely that later in responses T cells may rely on the ligase activity of Cbl-b to suppress TCR signaling which might include down-regulation of surface TCR-CD3 complex which is ubiquitination-dependent, as we and others have shown³⁵.

T cells in lymphoid organs are found to exhibit higher tonic signaling than those in the bloodstream⁸⁸. The continuous survey of self-pMHC provides tonic signals that are critical for the survival and functionality of naive T cells⁸⁹. Since treating resting T cells with the phosphatase inhibitor pervanadate leads to robust phosphorylation of multiple protein substrates, it has been proposed that basal signaling is a dynamic balance between kinases and phosphatases⁹⁰. The transmembrane receptor-like phosphatase CD45 maintains Lck in an active state by dephosphorylating Lck Y505 to provide support for its role in basal signaling, but also dephosphorylates Lck Y394, CD3 and ζ chains to inactivate them⁹¹.

While ZAP70 binds to phosphorylated ITAMs in the CD3 and ζ -chains in tonically signaling T cells⁹², whether this bound ZAP70 is catalytically active and signaling is unknown. Considering that ZAP70 kinase activity is required for STS1 recruitment by Cbl-b, it is unlikely that STS1 plays a major role in regulating tonic signaling in T cells. On the other hand, activated T cells produce lactic acid, acidifying the LNs and in tissues to suppress their own functions¹⁷. Thus, STS1 interaction with Cbl-b may be part of a negative feedback that modulates the intensity of the T cell response during the glycolytic shift in order to prevent immunopathology. Since STS1 phosphatase activity is required for the suppressive effects of low pH_e , this supports the idea that the regulatory function of STS1 is more evident in activated T cells where its catalytic activity is increased by the low pH_e established through the up-regulation of glycolysis.

The TME is known to be acidic²⁴, where T cell functions are largely suppressed. Treating a melanoma with a PPI neutralized TME acidity and restored T cell function, suggesting tumor acidity plays a critical role in immunosuppression²¹. Using the TRAMP-C2 prostate and melanoma tumor models, we demonstrated that inactivating *STS1* or *Cbl-b* significantly suppressed tumor growth and extended survival, accompanied by higher numbers of tumor-infiltrating T cells with more effector and stem-like properties and less exhaustion phenotypes. The rescue of T cell functions *in vivo* by deleting *STS1* strongly aligns with our *in vitro* assays, which demonstrated a significant improvement of T cell responsiveness under acidic pH_e . Although how deletion of *STS1* and *Cbl-b* leads to lower levels of exhaustion markers is unclear, the rescue of exhaustion phenotypes by targeting PD1 may depend on CD28 co-stimulation⁹³. Since *STS1*^{-/-} and *Cbl-b*^{-/-} T cells increase IL-2 secretion in a CD28-independent manner, this suggests their provision of a CD28-like signal in those T cells may counteract progression to exhaustion.

Inflamed tissues have also been found to be acidic, due to higher glucose consumption and lactic acid accumulation produced by activated immune cells^{94,95,96}. Interestingly, *STS1*^{-/-}/*STS2*^{-/-} mice are more resistant to *Candida Albicans* infection, shown by rapid pathogen clearance and enhanced survival^{46,97}. Due to conserved catalytic cores, it has been difficult to develop specific PTP inhibitors against conventional phosphatases. However, STS1 and STS2 are the only PTPs that use histidine, not cysteine in conventional PTPs⁴⁹. Crystallography also indicates that their catalytic cores are structurally distinct from conventional phosphatases⁹⁸. With STS2 being minimally active⁵⁰, the uniqueness of STS1 allows it to be specifically targeted for drug development to combat cancer and infection. Overall, our studies demonstrated a critical role of STS1 that allows T cells to sense and respond to acidic pH_e thereby tuning their own activation, which may have major impact on the physiological responses and pathological conditions.

LIMITATIONS OF THE STUDY

We attempted to understand how the phosphorylation of Y709 by ZAP70 at a distal region of Cbl-b impacted STS1 recruitment to a proximal proline-rich motif (aa 505 – 509). Due to the large sizes of Cbl-b and STS1, we were unable to produce enough of each protein with high purity for co-crystallization. Moreover, due to the large unstructured region of Cbl-b,

cryoEM and *in silico* modeling were not expected to generate meaningful results and were not pursued.

Our studies led us to investigate whether the autocrine effect of acid generated during T cell activation can occur *in vivo*. Although we attempted to down-regulate NHE1 using siRNA in primary OT-1 T cells followed by *in vivo* proliferation assay, these attempts were unsuccessful either due to ineffective siRNA molecules or unsuccessful siRNA transfection.

STAR★METHODS

RESOURCE AVAILABILITY

Lead Contact—Further information and requests for resources and reagents should be directed to and will be fulfilled by the lead contact, Arthur Weiss (Arthur.Weiss@ucsf.edu).

Materials Availability—Reagents generated in this study will be made available on request.

Data And Code Availability—This paper does not report original code. All data reported in this paper will be shared by the lead contact upon request.

EXPERIMENTAL MODEL AND SUBJECT DETAILS

Experimental animals—*STS1* and *STS2* doubly deficient mice were previously described and kindly provided by Dr. Nicholas Carpino at Stony Brook University⁴³. Singly deficient mice were obtained by breeding to wild-type C57BL/6 mice. *Cbl-b* deficient mice were previously described and kindly provided by Hua Gu³². These mice were housed in the pathogen-free facilities at the University of California, San Francisco (UCSF). Mice were treated according to the protocols approved by the UCSF veterinary committee and are in accordance with National Institutes of Health (NIH) guidelines. Both male and female mice at age 6–10 wk were used in the studies. For tumor studies 8–10-week-old mice were implanted subcutaneously with TRAMP-C2 (CRL-2731, ATCC) or B16-F10 tumor cells at a dosage of 1×10^6 cells or 1.25×10^5 cells, respectively, per mouse at the right flank. Tumors were measured twice a week with 3–4 days interval. Tumor volume was measured as $L \text{ (length)} \times W \text{ (width)} \times W / 2 \text{ (mm}^3\text{)}$, where the longer diameter was defined as length and the shorter diameter was defined as width. Mice were euthanized, once the tumor volume reached 2,000 mm³. For esomeprazole treatment, the day after when the tumor size reached 100 mm³, mice were injected intraperitoneally with esomeprazole at 12.5 mg/kg every other day for total 6 injections.

Cell culture—The human leukemic Jurkat T cell line and Jurkat variants were cultured in RPMI 1640 supplemented with 5% fetal bovine serum (FBS), 2 mM glutamine and 1% penicillin/streptomycin. Human embryonic kidney cell lines 293, 293T, murine melanoma cell line B16-F10 (CRL-6475, ATCC) and ovalbumin-expressing B16-F10 (kindly gifted by Dr. Matthew Krummel at the University of California, San Francisco) stable cell lines were cultured in DMEM containing 10% FBS, 1% penicillin/ streptomycin and 55 μM β -mercaptoethanol. TRAMP-C2 cells were cultured in DMEM containing 5%

FBS, 5% Nu-serum IV (Corning), 0.005 mg/mL bovine insulin (MilliporeSigma), 10 nM dehydroisoandrosterone (MilliporeSigma) and 1% penicillin/ streptomycin.

Primary cells were cultured in RPMI 1640 supplemented with 10% FBS, 2 mM glutamine, 1 mM sodium pyruvate, 5.6 mM KH₂PO₄, 1% penicillin/streptomycin, 20 mM HEPES and 55 μM β-mercaptoethanol. If needed, medium or PBS was then titrated at pH 6.6 with 0.1N HCl or pH 7.4 with 10N NaOH and filtered through 0.2 μm sterile membranes (MilliporeSigma). For TCR stimulation of Jurkat cells, cells were stimulated with IgM antibody clone C305 for 2 min for Western blot and immunoprecipitation, and 5 min for pErk detection by flow cytometry. For TCR stimulation in primary mouse T cells, cells were stimulated with Armenian hamster IgG clone 2C11 for 2 min followed by goat-anti-Armenian hamster antibodies for 2 min. For Src Family kinases inhibition, cells were treated with 10 μM PP2 5 min prior to TCR stimulation. For inhibition of Jurkat cells expressing analog-sensitive ZAP70, cells were treated with 10 μM 3-MB-PP1 5 min prior to TCR stimulation. For inhibition of protein synthesis, cells were treated with 100 μM cycloheximide for indicated time. For inhibition of NHE1, primary T cells were treated with 0.5 μM EIPA for 72 hr. For inhibition of H⁺-ATPase, primary T cells were treated with 5 μM esomeprazole for 72 hr.

METHOD DETAILS

Expression vector construction—Human *STS1* was PCR-amplified from Jurkat cDNA and cloned into pCDEF3 and pHR vectors, followed by T2A-mCherry. Human *STS1* mutants M47A, W295A and H391A were generated by site-directed mutagenesis (New England Biolabs). The cDNA sequence for SH3 domain of *STS1* (WT and W295A) was subcloned to pGEX 4T3 plasmid for the preparation of GST-fusion proteins. Human *Cbl-b*-expressing plasmid was gifted by Dr. Yun-Cai Liu (St. Jude's, Memphis), and subcloned to pCDEF3 and pHR vectors, followed by P2A-EGFP. Human *Cbl-b* mutants G298E, Y363F, C373A, Y665F, Y709F, Y889F, M940A, AVTSA, AAVAA, ACSGA, 430, 530, 630, 730 were generated by site-directed mutagenesis. Mouse *STS1*, *STS1-SHP1* chimera and *Cbl-b* were synthesized and cloned into pHR vectors using Gibson Assembly (New England Biolabs). Mouse *STS1* mutants W284A and H380A and *Cbl-b* mutants C373A and AAVAA were generated by site-directed mutagenesis. For CRISPR/Cas9 expressing vectors, targeting sequences for *STS1* (GCTCGGCATGGCTGCGAGAG), *c-Cbl* (TGGCCTGATTGGGCTCATGA) and *Cbl-b* (AGCAAGCTGCCGCAGATCGC) were ligated into the pX330 vector by T4 DNA ligase.

Electroporation— 2×10^7 Jurkat cells were resuspended in 400 μL serum-free medium and mixed with 20 μg DNA for expression vector transfection or 5 μg siRNA for siRNA transfection. Then cells were transferred to a Gene Pulser Cuvette (Bio-Rad) and electroporated at 1250 μF and 260 V by GenePulser Xcell (Bio-Rad). Cells were transferred to 6-well plates and added 10 mL medium. For vector transfected cells, cells were incubated 48 hr before experiments. For siRNA transfected cells, cells were incubated 72 hr before experiments.

Preparation of lentivirus— 2.5×10^6 293T cells were seeded in 10-cm dishes one day before the transfection of lentiviral vectors. On the next day, lentiviral vector pHR, pCMV dR8.91 and pMD2.G were transfected into 293T cells at ratio 4:3:1 by Turbofect transfection reagent (Invitrogen) following manufacturer's instructions. After 24 hr, cells were washed and cultured in 10 mL fresh RPMI 1640 medium. 48 hr later, supernatants were collected, and the viruses were concentrated using PEG-it (System Biosciences) following manufacturer's instructions and stored in -80°C .

Lentiviral transduction—For Jurkat cells, 3×10^6 Jurkat cells were resuspended in 1 mL fresh medium and mixed with concentrated virus. Cells were added to a 6-well plate and centrifuged at 2,500 rpm for 1 hr at room temperature. Then cells were added 5 mL fresh medium and kept at 37°C .

For primary T cells, isolated OT-1 CD8⁺ T cells were cultured in 24-well plates at 1×10^6 cells/mL and activated by mixing with anti-CD3/CD28 beads (Gibco) at $20 \mu\text{L}/1 \times 10^6$ cells for 2 days. Proliferating T cells were isolated using Percoll⁹⁹. After isolation, 1×10^6 cells were resuspended in 0.5 mL fresh medium supplemented with anti-CD3/CD28 beads and recombinant human IL-2 at 100 U/mL and mixed with concentrated virus. Cells were added to RetroNectin-coated at $20 \mu\text{g}/\text{mL}$ (Takara Bio) 6-well plate and centrifuged at 2,500 rpm for 1 hr at room temperature. Then the cells were incubated at 37°C and supplied with fresh medium after 24 hr.

Generation of Jurkat variants—For generating *STS1*^{-/-} and *Cbl-b*^{-/-} mutants, CRISPR/Cas9-mediated gene depletion was used. Briefly, CRISPR/Cas9 expressing vector pX330 encoding *STS1* or *Cbl-b*-targeting sequence were transfected into Jurkat cells via electroporation as described above. After 2 days, expression of Cas9 was selected by $1 \mu\text{g}/\text{mL}$ puromycin for 2 days. Cells were then plated at 0.5 cells per well in 96-well plates and expanded for 4 wk. Single clones were verified by sequencing and immunoblot. For *STS1*^{-/-}/*Cbl-b*^{-/-} mutants, *Cbl-b*^{-/-} mutant was transfected with CRISPR/Cas9 expressing vector pX330 encoding *STS1*-targeting sequence and selected as described above. For gene reconstitution of *STS1*^{-/-} or *Cbl-b*^{-/-} mutants, cells were infected with lentivirus encoding different WT and mutants of STS1 or Cbl-b with procedure described above. Reconstituted variants were sorted based on mCherry or EGFP fluorescence and verified by immunoblot.

In vitro phosphatase assay—The phosphatase activity under different pH conditions was determined using 6,8-difluoro-4-methylumbelliferyl phosphate (DifMUP; Thermo Fisher Scientific) as the substrate. The assay was performed as described⁵⁰, except the use of 100mM TAB buffer (20 mM Tris, 50 mM acetic acid, and 25 mM bis-Tris) titrated with 0.1N HCl and 10N NaOH to the desired pH, 150 mM NaCl, 0.1 mM EDTA and 0.1 μM of SHP1 (R&D systems), STS1 (Sino Biological) and STS2 (Sino Biological) phosphatase domains were used. Briefly, a 10X TAB buffer was diluted tenfold and fresh DTT was added to a final concentration of 1 mM. DifMUP was added from a freshly made 10 mM stock in DMSO. The final reaction contains 200 μM DifMUP and 0.1 μM phosphatase in total 100 μL . The mixtures were incubated at 37°C for 40 min. The reaction rate was measured by quantifying the fluorescence signaling of the product DifMU (excitation 360 nm, emission 450 nm) by FlexStation (Molecular Devices).

Intracellular pH (pH_i) measurement—Primary T cells were labeled with fluorescent pH-sensitive dye 2,7-biscarboxyethyl-5(6)-carboxyfluorescein (BCECF; Invitrogen). Briefly, cells were washed twice with HEPES buffer (25 mM HEPES pH 7.4, 140 mM NaCl, 5 mM KCl, 10 mM glucose, 1 mM MgSO₄, 2 mM CaCl₂). Cells were then labeled with BCECF in bicarbonate buffer (25 mM HCO₃ pH 7.4, 115 mM NaCl, 5 mM KCl, 10 mM glucose, 1 mM KPO₄, 1 mM MgSO₄, and 2 mM CaCl₂) at 1 × 10⁶ cells/mL 15 min at 37°C. Cells were washed twice by bicarbonate buffer and rested in bicarbonate buffer at desired pH, adjusted by 0.1N HCl, for 5 min at 37°C. 1.25 × 10⁵ primary T cells were used per well in a 96-well clear bottom plate in 100 μL bicarbonate buffer. Fluorescence of BCECF at Ex490/Em530 and Ex440/Em530 was acquired by FlexStation, and the fluorescence ratios were converted to pH_i by calibrating the fluorescence in each well with 10 μM nigericin.

Preparation of GST-fusion protein—The recombinant GST fused to STS1 SH3 domain was purified using Glutathione Sepharose 4B (Cytiva) and eluted following the manufacturer's instructions. Briefly, bacteria transformed with pGEX plasmids were cultured in 200 mL LB medium. When optical density at 600 nm (OD₆₀₀) reached 0.8, IPTG was added into the culture to 100 μM final concentration. Bacteria were cultured for 5 hr and collected by centrifugation at 3,500 rpm for 10 min at 4°C. Bacteria were resuspended in 10 mL ice-cold PBS containing 1% Triton, 1 mM PMSF, 1mM DTT and protease inhibitors 1 μg/mL leupeptin and 1 μg/mL pepstatin. Bacteria were lysed using sonication for 2 min on ice. Lysates were centrifuged at 14,000 ×g for 20 min at 4°C. Supernatants were collected and incubated with 200 μL Glutathione Sepharose 4B for 1 hr at room temperature with agitation. Beads were precipitated by centrifugation at 500 ×g for 5 min at 4°C. Beads were washed three times with 10 mL ice-cold PBS containing 1 mM PMSF, 1mM DTT and protease inhibitors 1 μg/mL leupeptin and 1 μg/mL pepstatin. beads were resuspended in 200 μL elution buffer (50 mM Tris-HCl pH 8.0) containing 10 mM reduced glutathione for 10 at room temperature to obtain GST fusion proteins.

Immunoblot analysis—Protein samples were subjected to 1.0 mm 8–12% SDS-PAGE (Invitrogen) and transferred to PVDF membranes using the 1.5MM GEL protocol of Trans-Blot Turbo Transfer System (Bio-Rad). Membranes were blocked by 5% BSA for 1 hr at room temperature, followed by incubation with primary antibodies at 1:1,000 dilution at 4°C on a rocker overnight. Membranes were washed 3 times with TBST and incubated with horseradish peroxidase conjugated secondary antibodies (Jackson ImmunoResearch) at 1:3,000 dilution for 1 hr at room temperature. Chemiluminescent signal was detected by ChemiDoc™ MP (Bio-Rad) and quantified by Image Lab (Bio-Rad).

Far-Western blot analysis—Protein samples were electrophoresed, transferred, and blocked as described above. Then the membranes were incubated with 5 μg recombinant GST fused to STS1 SH3 domain at 4°C on a rocker overnight. Membranes were washed 3 times with TBST and incubated with anti-GST antibody (1:1,000) for 1 hr at room temperature, followed by incubation with horseradish peroxidase conjugated secondary antibodies (1:1,000) for 1 hr at room temperature. Chemiluminescent signal was detected and analyzed as described above.

Immunoprecipitation—For Jurkat cells, 20×10^6 cells were stimulated by anti-TCR antibody (clone C305, Weiss lab) for 2 min at 37°C. For primary cells, 60×10^6 mouse CD4⁺ T cells were stimulated with biotinylated anti-CD3 (clone 2C11, eBioscience) for 2 min at 37°C, followed by streptavidin (Jackson ImmunoResearch) for 2 min at 37°C. Cells were then lysed in ice-cold NP-40 lysis buffer (1% NP-40 in PBS) supplemented with protease and phosphatase inhibitors (Roche). Lysates were centrifuged at 13,000 rpm for 10 min at 4°C. Supernatants were subjected to incubation with 5 μ L dynabeads (Life Technologies) and 1 μ g antibody at 4°C for 2 hr on a rotator. Beads were washed and eluted following the manufacturer's instructions. For immunoprecipitation against FLAG epitope, ANTI-FLAG M2 Affinity Gel (MilliporeSigma) was used following the manufacturer's instructions.

Flow cytometry— 1×10^6 single-cell suspensions from spleen, lymph nodes and thymus were incubated with anti-CD16/CD32 (Tonbo Biosciences) at 5 μ g/ml for 30 min on ice to block Fc receptors, together with surface markers. Dead cells were excluded using the LIVE/DEAD™ fixable, Violet, Near-IR death cell stain kit (Invitrogen) at 1:1,000 for 30 min on ice, or 4',6-diamidino-2-phenylindole (DAPI) (Thermo Fisher Scientific) at 1:5,000 in the FACS buffer after the final wash. For tumors, 5×10^6 cells were first incubated with Zombie Near-IR (ZIR) (Invitrogen) at 1:100 for 10 min in the dark, then washed with FACS Buffer. For specimens from mice challenged with TRAMP-C2 tumors, samples were incubated with 1:100 H-2D(b) Mouse 244–252 STHVNHLHC SPAS-1 tetramer (NIH Tetramer core) for 30 min at room temperature. After washing, surface staining including 1:50 Fc Block (Tonbo Biosciences) was performed for 30 min on ice. Cells were fixed using the eBioscience Foxp3 / Transcription Factor Staining Buffer Set (Life Technologies) and intracellular staining cocktail was finally added to samples for 30 min on ice before final wash with FACS Buffer.

Samples were run on a LSRFortessa (BD Biosciences). Data was analyzed by FlowJo 10.7 (BD Biosciences). Single cells were gated by FSC-A \times FSC-H and SSC-A \times SSC-H. Live cells were gated as live/dead fixable dye⁻ or DAPI⁻. CD8⁺ or CD4⁺ T cells were gated with CD3⁺, and CD8⁺ and CD4⁺, respectively. OT-1 and OT-2 cells were further gated with TCR V α 2⁺ with CD8⁺ and CD4⁺, respectively. Pmel-1 cells were further gated with TCR V β 13⁺ within CD8⁺. CD8⁺ or CD4⁺ infiltrating T cells for downstream marker analysis was gated from ZIR⁻CD45⁺CD3⁺ cells. Spas-1⁺ T cells were gated within CD8⁺.

TCR internalization assay— 0.5×10^6 splenocytes were resuspended in 50 μ L PBS containing Golgiplug (1:1,000) (BD Biosciences) to prevent the exocytosis of newly synthesized TCR/CD3 complex. Cells were stimulated by adding 50 μ L PBS containing anti-CD3 antibody (clone 2C11, Weiss lab) at final 1 μ g/mL for 2 min at 37°C with controls added at 4°C. Cells were crosslinked by adding 4 μ L biotinylated goat anti-hamster antibody (Jackson ImmunoResearch) at 37°C for controls at 4°C for 45 min. Cells were added 200 μ L ice-cold PBS and quenched on ice. Cells were centrifuged to remove supernatant and washed. Cells were stained by Alexa Fluor - 647 conjugated StreptAvidin to measure remaining surface CD3 by flow cytometry.

CD69 activation assay—For Jurkat cells, 1×10^6 Jurkat cells were cultured in 3 mL RPMI 1640 medium in anti-TCR antibody C305 (Weiss lab) coated 6-well plates (1:50,000 dilution) overnight at 37°C. For primary cells, 0.1×10^6 OT-1 T cells were co-cultured in 100 uL RPMI 1640 medium with antigen-presenting cells (APCs) from $\text{Ca}^{-/-}$ mice at 1:5 ratio with different concentrations of OVA peptides overnight at 37°C. 0.1×10^6 Pmel-1 T cells were co-cultured in 100 uL RPMI 1640 medium with APCs from $\text{Ca}^{-/-}$ mice at 1:5 ratio with mouse gp100 (mgp100) peptide at 10^{-11} M overnight at 37°C.

Phospho-Erk activation assay— 1×10^6 Jurkat cells in 100 uL were stimulated by anti-TCR antibody C305 ascites (Weiss lab) at 1:1,000 for 5 min. Then cells were fixed by PBS/BD Cytotfix™ Fixation Buffer (BD Biosciences) (1:1 v/v) for 15 min. Cells were washed with FACS buffer and permeabilized by 90% methanol at -20°C overnight. Cells were washed and added anti-phospho-Erk antibody (Cell Signaling) for 45 min at room temperature, followed by Alexa Fluor - 647-conjugated goat anti-rabbit antibodies (Jackson ImmunoResearch) at 1:2,000 for 30 min at room temperature. Cells were washed and subjected to flow cytometry.

Cytokine secretion assay—Cultured cells were added Golgiplug (BD Biosciences) following manufacturer's instructions for 4 hr. Cells were washed by FACS buffer and labeled in the presence of Golgiplug. Then cells were fixed by PBS/BD Cytotfix™ Fixation Buffer (BD Biosciences) (1:1 v/v) for 15 min. Cells were washed with FACS buffer and permeabilized by 90% methanol at -20°C overnight. Cells were washed and labeled with fluorescence-conjugated antibodies against cytokines for 45 min at room temperature. Cells were washed and subjected to flow cytometry.

In vitro proliferation assay—Isolated T cells were labeled with CellTrace Violet (Thermo Fisher Scientific) following manufacturer's instructions. 0.2×10^6 cells in 0.2 mL were added to each well of anti-CD3 antibody (clone 2C11, Weiss lab) coated flat-bottom 96-well plates and incubated in 37°C for 3 days. Fluorescent signal of CellTrace Violet was detected by flow cytometry.

In vivo proliferation assay—Isolated OT-1 T cells were labeled with CellTrace Violet or Yellow (Thermo Fisher Scientific) following manufacturer's instructions. Cells were adoptively transferred into BoyJ mice at 1:1 ratio with total 2×10^6 cells. After 24 hr, mice were injected with 5 $\mu\text{g}/50$ uL ovalbumin/complete freund's adjuvant (1:1 v/v) in the footpad. 3 days later, draining and contralateral lymph nodes were excised, and the proliferation of labeled OT-1 T cells were analyzed by flow cytometry.

In vivo differentiation assay—Isolated OT-2 T cells were adoptively transferred into BoyJ mice with total 1×10^6 cells. After 24 hr, mice were injected with 50 $\mu\text{g}/50$ uL ovalbumin/complete freund's adjuvant (1:1 v/v) in the right flank subcutaneously. 10 days later, draining and contralateral lymph nodes were excised, and the differentiation of OT-2 T cells were analyzed by flow cytometry.

In vivo labeling using pH Low insertion peptide (pHLIP)—The pHLIP peptide (AEQNPIYWARYADWLFTPLLLLDLALLVDADEGT) was conjugated to Cy5 at the N-

terminus and synthesized (GenScript). For detection by flow cytometry, 50 μ L Cy5-pHLIP peptide (1 mg/mL) was injected in the hock 5 hr prior to harvest. For *in vivo* imaging, mice were injected intraperitoneally with Cy5-pHLIP peptide at a dose of 0.5 mg/kg. After 24 hr, mouse right flanks were shaved and fluorescence intensity at the 680 nm range in the tumor area was measured by IVIS Spectrum (Xenogen). Images were processed with the Living Image (Xenogen) and ImageJ.

***In vitro* cytolytic assay**—For target cell preparation, 5×10^4 ovalbumin-expressing B16-F10 cells in 1 mL were seeded in 24-wells and waited for the cells to fully adhere prior to the addition of cytolytic T cells. For cytolytic T cell preparation, splenocytes from OT-1 mice were re-suspended at 4×10^6 cells/mL and stimulated with OVA peptide in total 5 mL in 6-well plates for 3 days. Cells were supplemented with fresh medium containing final concentration of recombinant human IL-2 at 100 U/mL for 4 days. Differentiated cytotoxic T cells were isolated by histopaque 1083 (MilliporeSigma) following manufacturer's instructions. Cytolytic T cells were added into B16 cell-containing 24-well plates at different ratios to B16-F10 cells with 100 U/mL recombinant human IL-2 and incubated at 37°C for 3 days. Then cells were collected and stained with LIVE/DEAD™ Violet (Thermo Fisher Scientific) and cell viability were analyzed by flow cytometry.

Tissue processing for immunophenotyping of tumor models—Tumors and lymph nodes were surgically removed with sterilized equipment. Lymph nodes were crushed between two super-frosted microscope slides and washed into wells of 6-well plates containing cold PBS. TILs were isolated as previously described¹⁰⁰. Briefly, tumors were minced with scalpel blades and digested to single cell suspensions by incubation for 1 hr at 37°C in tumor digestion media containing DMEM, 10% FBS, 2 mg/ml Collagenase IV (Sigma-Aldrich) and DNase I (Sigma-Aldrich). Then, tumor lysates were filtered through a 100 μ m filter into 50 mL conical tubes and filled with cold PBS. Tissue single cell lysates were centrifuged at 450 \times g for 5 min at 4°C. Supernatants were discarded and pellets were resuspended in 5 mL ACK Lysis Buffer (Quality Biological), mixed well and kept on ice for 5 min. Lysis was stopped by filling the tubes with cold PBS. Samples were centrifuged again and finally resuspended in 1 mL cold PBS. Viable cells for downstream use were counted in a Vi-CELL (Beckman Coulter) at a 1:60 dilution.

Enzyme-linked immunosorbent assay (ELISA)—Secreted cytokines were detected using BD OptEIA™ Mouse kits (BD Biosciences) following manufacturer's instructions.

Sequence alignments and analysis—Sequences of Cbl-b orthologs from various mammals were identified and aligned via UniProt. The sequences surrounding the proline-rich region PPVPP and Y709 across all orthologs were picked out and their degrees of evolutionary conservation were visualized using WebLogo¹⁰¹.

High-throughput peptide phosphorylation and binding screens—The results presented in this study were obtained from a database generated using a previously established procedure⁵⁷ without any modifications.

QUANTIFICATION AND STATISTICAL ANALYSIS

Statistical Analysis—GraphPad Prism 7 Software (GraphPad Software) was used for data analysis and representation. Statistical analysis was applied to biological replicates, or biologically independent mice for each experiment. All experiments described in this study have been performed at least two times. For comparisons > 2 groups, one-way ANOVA was applied. For comparison between 2 groups, two-tailed Student's *t* test was applied. Survival curves comparing wild-type versus each mutant were analyzed by log-rank test. Tumor growth curves among groups were analyzed by two-way ANOVA comparison among groups. Error bars represent standard deviation. *p*-values less than 0.05 were considered statistically significant. **p* < 0.05, ***p* < 0.01, ****p* < 0.005.

Supplementary Material

Refer to Web version on PubMed Central for supplementary material.

ACKNOWLEDGMENTS

We thank A. Roque (University of California, San Francisco) (UCSF) for animal husbandry; B. Au-Yeung (Emory University), A. Courtney (University of Michigan), J. Zikherman (UCSF) for critical feedback; W. Lu, L. Shen, J. Brooks (UCSF) for research advice; NIH Tetramer Core Facility for providing the Spas-1 MHC class I tetramer. The work was supported by the Howard Hughes Medical Institute (A.W. and J.K.), NIAID P01 AI091580 (A.W.), NCI R35 CA253175 (L.F.), T32 CA108462–17 (Y.L.T.), Cancer Research Institute Irvington Postdoctoral Fellowship (Y.L.T.), Damon Runyon Cancer Research Foundation Fellowship (N.H.S.), and Prostate Cancer Foundation Challenge Award (L.F.).

REFERENCES

- Iwashima M, Irving BA, van Oers NS, Chan AC, and Weiss A (1994). Sequential interactions of the TCR with two distinct cytoplasmic tyrosine kinases. *Science* 263, 1136–1139. 10.1126/science.7509083. [PubMed: 7509083]
- Courtney AH, Lo WL, and Weiss A (2018). TCR Signaling: Mechanisms of Initiation and Propagation. *Trends Biochem Sci* 43, 108–123. 10.1016/j.tibs.2017.11.008. [PubMed: 29269020]
- Gaud G, Lesourne R, and Love PE (2018). Regulatory mechanisms in T cell receptor signalling. *Nat Rev Immunol* 18, 485–497. 10.1038/s41577-018-0020-8. [PubMed: 29789755]
- Mandl JN, Monteiro JP, Vriskoop N, and Germain RN (2013). T cell-positive selection uses self-ligand binding strength to optimize repertoire recognition of foreign antigens. *Immunity* 38, 263–274. 10.1016/j.immuni.2012.09.011. [PubMed: 23290521]
- Zinzow-Kramer WM, Weiss A, and Au-Yeung BB (2019). Adaptation by naive CD4(+) T cells to self-antigen-dependent TCR signaling induces functional heterogeneity and tolerance. *Proc Natl Acad Sci U S A* 116, 15160–15169. 10.1073/pnas.1904096116. [PubMed: 31285342]
- Cooper JA, Kaneko T, and Li SS (2015). Cell regulation by phosphotyrosine-targeted ubiquitin ligases. *Mol Cell Biol* 35, 1886–1897. 10.1128/MCB.00098-15. [PubMed: 25776560]
- Zhang W, Tribble RP, Zhu M, Liu SK, McGlade CJ, and Samelson LE (2000). Association of Grb2, Gads, and phospholipase C-gamma 1 with phosphorylated LAT tyrosine residues. Effect of LAT tyrosine mutations on T cell antigen receptor-mediated signaling. *J Biol Chem* 275, 23355–23361. 10.1074/jbc.M000404200. [PubMed: 10811803]
- Ganti RS, Lo WL, McAfee DB, Groves JT, Weiss A, and Chakraborty AK (2020). How the T cell signaling network processes information to discriminate between self and agonist ligands. *Proc Natl Acad Sci U S A* 117, 26020–26030. 10.1073/pnas.2008303117. [PubMed: 33020303]
- Lo WL, Shah NH, Rubin SA, Zhang W, Horkova V, Fallahee IR, Stepanek O, Zon LI, Kuriyan J, and Weiss A (2019). Slow phosphorylation of a tyrosine residue in LAT optimizes T cell ligand discrimination. *Nat Immunol* 20, 1481–1493. 10.1038/s41590-019-0502-2. [PubMed: 31611699]

10. Voisinne G, Locard-Paulet M, Froment C, Maturin E, Menoita MG, Girard L, Mellado V, Burlet-Schiltz O, Malissen B, Gonzalez de Peredo A, and Roncagalli R (2022). Kinetic proofreading through the multi-step activation of the ZAP70 kinase underlies early T cell ligand discrimination. *Nat Immunol* 23, 1355–1364. 10.1038/s41590-022-01288-x. [PubMed: 36045187]
11. Okazaki T, and Honjo T (2006). The PD-1-PD-L pathway in immunological tolerance. *Trends Immunol* 27, 195–201. 10.1016/j.it.2006.02.001. [PubMed: 16500147]
12. Nguyen TTT, Wang ZE, Shen L, Schroeder A, Eckalbar W, and Weiss A (2021). Cbl-b deficiency prevents functional but not phenotypic T cell anergy. *J Exp Med* 218. 10.1084/jem.20202477.
13. Lutz-Nicoladoni C, Wolf D, and Sopper S (2015). Modulation of Immune Cell Functions by the E3 Ligase Cbl-b. *Front Oncol* 5, 58. 10.3389/fonc.2015.00058. [PubMed: 25815272]
14. Bardhan K, Anagnostou T, and Boussiotis VA (2016). The PD1:PD-L1/2 Pathway from Discovery to Clinical Implementation. *Front Immunol* 7, 550. 10.3389/fimmu.2016.00550. [PubMed: 28018338]
15. Hui E, Cheung J, Zhu J, Su X, Taylor MJ, Wallweber HA, Sasmal DK, Huang J, Kim JM, Mellman I, and Vale RD (2017). T cell costimulatory receptor CD28 is a primary target for PD-1-mediated inhibition. *Science* 355, 1428–1433. 10.1126/science.aaf1292. [PubMed: 28280247]
16. Johnston RJ, Su LJ, Pinckney J, Critton D, Boyer E, Krishnakumar A, Corbett M, Rankin AL, Dibella R, Campbell L, et al. (2019). VISTA is an acidic pH-selective ligand for PSGL-1. *Nature* 574, 565–570. 10.1038/s41586-019-1674-5. [PubMed: 31645726]
17. Wu H, Estrella V, Beatty M, Abrahams D, El-Kenawi A, Russell S, Ibrahim-Hashim A, Longo DL, Reshetnyak YK, Moshnikova A, et al. (2020). T-cells produce acidic niches in lymph nodes to suppress their own effector functions. *Nat Commun* 11, 4113. 10.1038/s41467-020-17756-7. [PubMed: 32807791]
18. Concepcion AR, Salas JT, Sarvide S, Saez E, Ferrer A, Lopez M, Portu A, Banales JM, Hervás-Stubbbs S, Oude Elferink RP, et al. (2014). Anion exchanger 2 is critical for CD8(+) T cells to maintain pH homeostasis and modulate immune responses. *Eur J Immunol* 44, 1341–1351. 10.1002/eji.201344218. [PubMed: 24515893]
19. Concepcion AR, Salas JT, Saez E, Sarvide S, Ferrer A, Portu A, Uriarte I, Hervás-Stubbbs S, Oude Elferink RP, Prieto J, and Medina JF (2015). CD8+ T cells undergo activation and programmed death-1 repression in the liver of aged Ae2a,b^{-/-} mice favoring autoimmune cholangitis. *Oncotarget* 6, 28588–28606. 10.18632/oncotarget.5665. [PubMed: 26396175]
20. Boron WF (2004). Regulation of intracellular pH. *Adv Physiol Educ* 28, 160–179. 10.1152/advan.00045.2004. [PubMed: 15545345]
21. Calcinotto A, Filipazzi P, Grioni M, Iero M, De Milito A, Ricupito A, Cova A, Canese R, Jachetti E, Rossetti M, et al. (2012). Modulation of microenvironment acidity reverses anergy in human and murine tumor-infiltrating T lymphocytes. *Cancer Res* 72, 2746–2756. 10.1158/0008-5472.CAN-11-1272. [PubMed: 22593198]
22. Nakagawa Y, Negishi Y, Shimizu M, Takahashi M, Ichikawa M, and Takahashi H (2015). Effects of extracellular pH and hypoxia on the function and development of antigen-specific cytotoxic T lymphocytes. *Immunol Lett* 167, 72–86. 10.1016/j.imlet.2015.07.003. [PubMed: 26209187]
23. Pilon-Thomas S, Kodumudi KN, El-Kenawi AE, Russell S, Weber AM, Luddy K, Damaghi M, Wojtkowiak JW, Mule JJ, Ibrahim-Hashim A, and Gillies RJ (2016). Neutralization of Tumor Acidity Improves Antitumor Responses to Immunotherapy. *Cancer Res* 76, 1381–1390. 10.1158/0008-5472.CAN-15-1743. [PubMed: 26719539]
24. Bader JE, Voss K, and Rathmell JC (2020). Targeting Metabolism to Improve the Tumor Microenvironment for Cancer Immunotherapy. *Mol Cell* 78, 1019–1033. 10.1016/j.molcel.2020.05.034. [PubMed: 32559423]
25. Buck MD, Sowell RT, Kaech SM, and Pearce EL (2017). Metabolic Instruction of Immunity. *Cell* 169, 570–586. 10.1016/j.cell.2017.04.004. [PubMed: 28475890]
26. Chiang JY, Jang IK, Hodes R, and Gu H (2007). Ablation of Cbl-b provides protection against transplanted and spontaneous tumors. *J Clin Invest* 117, 1029–1036. 10.1172/JCI29472. [PubMed: 17364027]

27. Loeser S, Loser K, Bijker MS, Rangachari M, van der Burg SH, Wada T, Beissert S, Melief CJ, and Penninger JM (2007). Spontaneous tumor rejection by cbl-b-deficient CD8+ T cells. *J Exp Med* 204, 879–891. 10.1084/jem.20061699. [PubMed: 17403934]
28. Schmidt MHH, and Dikic I (2005). The Cbl interactome and its functions. *Nat Rev Mol Cell Biol* 6, 907–918. 10.1038/nrm1762. [PubMed: 16227975]
29. Murphy MA, Schnall RG, Venter DJ, Barnett L, Bertoncello I, Thien CB, Langdon WY, and Bowtell DD (1998). Tissue hyperplasia and enhanced T-cell signalling via ZAP-70 in c-Cbl-deficient mice. *Mol Cell Biol* 18, 4872–4882. 10.1128/MCB.18.8.4872. [PubMed: 9671496]
30. Naramura M, Kole HK, Hu RJ, and Gu H (1998). Altered thymic positive selection and intracellular signals in Cbl-deficient mice. *Proc Natl Acad Sci U S A* 95, 15547–15552. 10.1073/pnas.95.26.15547. [PubMed: 9861006]
31. Bachmaier K, Krawczyk C, Kozieradzki I, Kong YY, Sasaki T, Oliveira-dos-Santos A, Mariathasan S, Bouchard D, Wakeham A, Itie A, et al. (2000). Negative regulation of lymphocyte activation and autoimmunity by the molecular adaptor Cbl-b. *Nature* 403, 211–216. 10.1038/35003228. [PubMed: 10646608]
32. Chiang YJ, Kole HK, Brown K, Naramura M, Fukuhara S, Hu RJ, Jang IK, Gutkind JS, Shevach E, and Gu H (2000). Cbl-b regulates the CD28 dependence of T-cell activation. *Nature* 403, 216–220. 10.1038/35003235. [PubMed: 10646609]
33. Thien CB, and Langdon WY (2001). Cbl: many adaptations to regulate protein tyrosine kinases. *Nat Rev Mol Cell Biol* 2, 294–307. 10.1038/35067100. [PubMed: 11283727]
34. Myers MD, Sosinowski T, Dragone LL, White C, Band H, Gu H, and Weiss A (2006). Src-like adaptor protein regulates TCR expression on thymocytes by linking the ubiquitin ligase c-Cbl to the TCR complex. *Nat Immunol* 7, 57–66. 10.1038/ni1291. [PubMed: 16327786]
35. Naramura M, Jang IK, Kole H, Huang F, Haines D, and Gu H (2002). c-Cbl and Cbl-b regulate T cell responsiveness by promoting ligand-induced TCR down-modulation. *Nat Immunol* 3, 1192–1199. 10.1038/ni855. [PubMed: 12415267]
36. Pierce NW, Kleiger G, Shan SO, and Deshaies RJ (2009). Detection of sequential polyubiquitylation on a millisecond timescale. *Nature* 462, 615–619. 10.1038/nature08595. [PubMed: 19956254]
37. Rao N, Lupher ML Jr., Ota S, Reedquist KA, Druker BJ, and Band H (2000). The linker phosphorylation site Tyr292 mediates the negative regulatory effect of Cbl on ZAP-70 in T cells. *J Immunol* 164, 4616–4626. [PubMed: 10779765]
38. Thien CB, Bowtell DD, and Langdon WY (1999). Perturbed regulation of ZAP-70 and sustained tyrosine phosphorylation of LAT and SLP-76 in c-Cbl-deficient thymocytes. *J Immunol* 162, 7133–7139. [PubMed: 10358158]
39. Balagopalan L, Barr VA, Sommers CL, Barda-Saad M, Goyal A, Isakowitz MS, and Samelson LE (2007). c-Cbl-mediated regulation of LAT-nucleated signaling complexes. *Mol Cell Biol* 27, 8622–8636. 10.1128/MCB.00467-07. [PubMed: 17938199]
40. Tsygankov AY (2009). TULA-family proteins: an odd couple. *Cell Mol Life Sci* 66, 2949–2952. 10.1007/s00018-009-0071-x. [PubMed: 19585081]
41. Chen Y, Jakoncic J, Carpino N, and Nassar N (2009). Structural and functional characterization of the 2H-phosphatase domain of Sts-2 reveals an acid-dependent phosphatase activity. *Biochemistry* 48, 1681–1690. 10.1021/bi802219n. [PubMed: 19196006]
42. Kowanetz K, Crosetto N, Haglund K, Schmidt MHH, Heldin CH, and Dikic I (2004). Suppressors of T-cell receptor signaling Sts-1 and Sts-2 bind to Cbl and inhibit endocytosis of receptor tyrosine kinases. *J Biol Chem* 279, 32786–32795. 10.1074/jbc.M403759200. [PubMed: 15159412]
43. Carpino N, Turner S, Mekala D, Takahashi Y, Zang H, Geiger TL, Doherty P, and Ihle JN (2004). Regulation of ZAP-70 activation and TCR signaling by two related proteins, Sts-1 and Sts-2. *Immunity* 20, 37–46. [PubMed: 14738763]
44. Carpino N, Chen Y, Nassar N, and Oh HW (2009). The Sts proteins target tyrosine phosphorylated, ubiquitinated proteins within TCR signaling pathways. *Mol Immunol* 46, 3224–3231. 10.1016/j.molimm.2009.08.015. [PubMed: 19733910]

45. Parashar K, Kopping E, Frank D, Sampath V, Thanassi DG, and Carpino N (2017). Increased Resistance to Intradermal *Francisella tularensis* LVS Infection by Inactivation of the Sts Phosphatases. *Infect Immun* 85. 10.1128/IAI.00406-17.
46. Naseem S, Frank D, Konopka JB, and Carpino N (2015). Protection from systemic *Candida albicans* infection by inactivation of the Sts phosphatases. *Infect Immun* 83, 637–645. 10.1128/IAI.02789-14. [PubMed: 25422266]
47. Cieniewicz B, Carpino N, and Krug LT (2014). Enhanced response of T cells from murine gammaherpesvirus 68-infected mice lacking the suppressor of T cell receptor signaling molecules Sts-1 and Sts-2. *PLoS One* 9, e90196. 10.1371/journal.pone.0090196. [PubMed: 24587276]
48. Voisinne G, Garcia-Blesa A, Chaoui K, Fiore F, Bergot E, Girard L, Malissen M, Burlet-Schiltz O, Gonzalez de Peredo A, Malissen B, and Roncagalli R (2016). Co-recruitment analysis of the CBL and CBLB signalosomes in primary T cells identifies CD5 as a key regulator of TCR-induced ubiquitylation. *Mol Syst Biol* 12, 876. 10.15252/msb.20166837. [PubMed: 27474268]
49. Guan KL, and Dixon JE (1991). Evidence for protein-tyrosine-phosphatase catalysis proceeding via a cysteine-phosphate intermediate. *J Biol Chem* 266, 17026–17030. [PubMed: 1654322]
50. Zhou W, Yin Y, Weinheimer AS, Kaur N, Carpino N, and French JB (2017). Structural and Functional Characterization of the Histidine Phosphatase Domains of Human Sts-1 and Sts-2. *Biochemistry* 56, 4637–4645. 10.1021/acs.biochem.7b00638. [PubMed: 28759203]
51. Kumar M, Michael S, Alvarado-Valverde J, Meszaros B, Samano-Sanchez H, Zeke A, Dobson L, Lazar T, Ord M, Nagpal A, et al. (2022). The Eukaryotic Linear Motif resource: 2022 release. *Nucleic Acids Res* 50, D497–D508. 10.1093/nar/gkab975. [PubMed: 34718738]
52. Kobashigawa Y, Tomitaka A, Kumeta H, Noda NN, Yamaguchi M, and Inagaki F (2011). Autoinhibition and phosphorylation-induced activation mechanisms of human cancer and autoimmune disease-related E3 protein Cbl-b. *Proc Natl Acad Sci U S A* 108, 20579–20584. 10.1073/pnas.1110712108. [PubMed: 22158902]
53. Levin SE, Zhang C, Kadlec TA, Shokat KM, and Weiss A (2008). Inhibition of ZAP-70 kinase activity via an analog-sensitive allele blocks T cell receptor and CD28 superagonist signaling. *J Biol Chem* 283, 15419–15430. 10.1074/jbc.M709000200. [PubMed: 18378687]
54. Zhang Z, Elly C, Qiu L, Altman A, and Liu YC (1999). A direct interaction between the adaptor protein Cbl-b and the kinase zap-70 induces a positive signal in T cells. *Curr Biol* 9, 203–206. 10.1016/s0960-9822(99)80090-6. [PubMed: 10074432]
55. Peschard P, Kozlov G, Lin T, Mirza IA, Berghuis AM, Lipkowitz S, Park M, and Gehring K (2007). Structural basis for ubiquitin-mediated dimerization and activation of the ubiquitin protein ligase Cbl-b. *Mol Cell* 27, 474–485. 10.1016/j.molcel.2007.06.023. [PubMed: 17679095]
56. Shah NH, Wang Q, Yan Q, Karandur D, Kadlec TA, Fallahee IR, Russ WP, Ranganathan R, Weiss A, and Kuriyan J (2016). An electrostatic selection mechanism controls sequential kinase signaling downstream of the T cell receptor. *Elife* 5. 10.7554/eLife.20105.
57. Shah NH, Lobel M, Weiss A, and Kuriyan J (2018). Fine-tuning of substrate preferences of the Src-family kinase Lck revealed through a high-throughput specificity screen. *Elife* 7. 10.7554/eLife.35190.
58. San Luis B, Sondgeroth B, Nassar N, and Carpino N (2011). Sts-2 is a phosphatase that negatively regulates zeta-associated protein (ZAP)-70 and T cell receptor signaling pathways. *J Biol Chem* 286, 15943–15954. 10.1074/jbc.M110.177634. [PubMed: 21393235]
59. Han J, and Burgess K (2010). Fluorescent indicators for intracellular pH. *Chem Rev* 110, 2709–2728. 10.1021/cr900249z. [PubMed: 19831417]
60. Erra Diaz F, Dantas E, and Geffner J (2018). Unravelling the Interplay between Extracellular Acidosis and Immune Cells. *Mediators Inflamm* 2018, 1218297. 10.1155/2018/1218297. [PubMed: 30692870]
61. Kruisbeek AM, Shevach E, and Thornton AM (2004). Proliferative assays for T cell function. *Curr Protoc Immunol* Chapter 3, Unit 3 12. 10.1002/0471142735.im0312s60.
62. Jenkins MK, Chen CA, Jung G, Mueller DL, and Schwartz RH (1990). Inhibition of antigen-specific proliferation of type 1 murine T cell clones after stimulation with immobilized anti-CD3 monoclonal antibody. *J Immunol* 144, 16–22. [PubMed: 2153162]

63. Daniels MA, Teixeira E, Gill J, Hausmann B, Roubaty D, Holmberg K, Werlen G, Hollander GA, Gascoigne NR, and Palmer E (2006). Thymic selection threshold defined by compartmentalization of Ras/MAPK signalling. *Nature* 444, 724–729. 10.1038/nature05269. [PubMed: 17086201]
64. Paolino M, Thien CB, Gruber T, Hinterleitner R, Baier G, Langdon WY, and Penninger JM (2011). Essential role of E3 ubiquitin ligase activity in Cbl-b-regulated T cell functions. *J Immunol* 186, 2138–2147. 10.4049/jimmunol.1003390. [PubMed: 21248250]
65. Menk AV, Scharping NE, Moreci RS, Zeng X, Guy C, Salvatore S, Bae H, Xie J, Young HA, Wendell SG, and Delgoffe GM (2018). Early TCR Signaling Induces Rapid Aerobic Glycolysis Enabling Distinct Acute T Cell Effector Functions. *Cell Rep* 22, 1509–1521. 10.1016/j.celrep.2018.01.040. [PubMed: 29425506]
66. Webb BA, White KA, Grillo-Hill BK, Schonichen A, Choi C, and Barber DL (2016). A Histidine Cluster in the Cytoplasmic Domain of the Na-H Exchanger NHE1 Confers pH-sensitive Phospholipid Binding and Regulates Transporter Activity. *J Biol Chem* 291, 24096–24104. 10.1074/jbc.M116.736215. [PubMed: 27650500]
67. Reshetnyak YK, Andreev OA, Segala M, Markin VS, and Engelman DM (2008). Energetics of peptide (pHLIP) binding to and folding across a lipid bilayer membrane. *Proc Natl Acad Sci U S A* 105, 15340–15345. 10.1073/pnas.0804746105. [PubMed: 18829441]
68. Tapmeier TT, Moshnikova A, Beech J, Allen D, Kinches P, Smart S, Harris A, McIntyre A, Engelman DM, Andreev OA, et al. (2015). The pH low insertion peptide pHLIP Variant 3 as a novel marker of acidic malignant lesions. *Proc Natl Acad Sci U S A* 112, 9710–9715. 10.1073/pnas.1509488112. [PubMed: 26195776]
69. Narayanan T, Weerakkody D, Karabadzak AG, Anderson M, Andreev OA, and Reshetnyak YK (2016). pHLIP Peptide Interaction with a Membrane Monitored by SAXS. *J Phys Chem B* 120, 11484–11491. 10.1021/acs.jpcc.6b06643. [PubMed: 27726396]
70. Ibrahim-Hashim A, Cornell HH, Abrahams D, Lloyd M, Bui M, Gillies RJ, and Gatenby RA (2012). Systemic buffers inhibit carcinogenesis in TRAMP mice. *J Urol* 188, 624–631. 10.1016/j.juro.2012.03.113. [PubMed: 22704445]
71. Korenchan DE, Flavell RR, Baligand C, Sriram R, Neumann K, Sukumar S, VanBrocklin H, Vigneron DB, Wilson DM, and Kurhanewicz J (2016). Dynamic nuclear polarization of biocompatible (¹³C)-enriched carbonates for in vivo pH imaging. *Chem Commun (Camb)* 52, 3030–3033. 10.1039/c5cc09724j. [PubMed: 26792559]
72. Korenchan DE, Bok R, Sriram R, Liu K, Santos RD, Qin H, Lobach I, Korn N, Wilson DM, Kurhanewicz J, and Flavell RR (2019). Hyperpolarized in vivo pH imaging reveals grade-dependent acidification in prostate cancer. *Oncotarget* 10, 6096–6110. 10.18632/oncotarget.27225. [PubMed: 31692908]
73. Chen Z, Ji Z, Ngiow SF, Manne S, Cai Z, Huang AC, Johnson J, Staube RP, Bengsch B, Xu C, et al. (2019). TCF-1-Centered Transcriptional Network Drives an Effector versus Exhausted CD8 T Cell-Fate Decision. *Immunity* 51, 840–855 e845. 10.1016/j.immuni.2019.09.013. [PubMed: 31606264]
74. Wu T, Ji Y, Moseman EA, Xu HC, Manglani M, Kirby M, Anderson SM, Handon R, Kenyon E, Elkhahloun A, et al. (2016). The TCF1-Bcl6 axis counteracts type I interferon to repress exhaustion and maintain T cell stemness. *Sci Immunol* 1. 10.1126/sciimmunol.aai8593.
75. Utzschneider DT, Charmoy M, Chennupati V, Pousse L, Ferreira DP, Calderon-Copete S, Danilo M, Alfei F, Hofmann M, Wieland D, et al. (2016). T Cell Factor 1-Expressing Memory-like CD8(+) T Cells Sustain the Immune Response to Chronic Viral Infections. *Immunity* 45, 415–427. 10.1016/j.immuni.2016.07.021. [PubMed: 27533016]
76. Chen LQ, and Pagel MD (2015). Evaluating pH in the Extracellular Tumor Microenvironment Using CEST MRI and Other Imaging Methods. *Adv Radiol* 2015. 10.1155/2015/206405.
77. Overwijk WW, Theoret MR, Finkelstein SE, Surman DR, de Jong LA, Vyth-Dreese FA, DelleMijn TA, Antony PA, Spiess PJ, Palmer DC, et al. (2003). Tumor regression and autoimmunity after reversal of a functionally tolerant state of self-reactive CD8+ T cells. *J Exp Med* 198, 569–580. 10.1084/jem.20030590. [PubMed: 12925674]
78. Reshetnyak YK, Moshnikova A, Andreev OA, and Engelman DM (2020). Targeting Acidic Diseased Tissues by pH-Triggered Membrane-Associated Peptide Folding. *Front Bioeng Biotechnol* 8, 335. 10.3389/fbioe.2020.00335. [PubMed: 32411684]

79. Webb BA, Chimenti M, Jacobson MP, and Barber DL (2011). Dysregulated pH: a perfect storm for cancer progression. *Nat Rev Cancer* 11, 671–677. 10.1038/nrc3110. [PubMed: 21833026]
80. Haynes C, Oldfield CJ, Ji F, Klitgord N, Cusick ME, Radivojac P, Uversky VN, Vidal M, and Iakoucheva LM (2006). Intrinsic disorder is a common feature of hub proteins from four eukaryotic interactomes. *PLoS Comput Biol* 2, e100. 10.1371/journal.pcbi.0020100. [PubMed: 16884331]
81. Wright PE, and Dyson HJ (2015). Intrinsically disordered proteins in cellular signalling and regulation. *Nat Rev Mol Cell Biol* 16, 18–29. 10.1038/nrm3920. [PubMed: 25531225]
82. Bah A, and Forman-Kay JD (2016). Modulation of Intrinsically Disordered Protein Function by Post-translational Modifications. *J Biol Chem* 291, 6696–6705. 10.1074/jbc.R115.695056. [PubMed: 26851279]
83. Berlow RB, Dyson HJ, and Wright PE (2018). Expanding the Paradigm: Intrinsically Disordered Proteins and Allosteric Regulation. *J Mol Biol* 430, 2309–2320. 10.1016/j.jmb.2018.04.003. [PubMed: 29634920]
84. Iakoucheva LM, Radivojac P, Brown CJ, O'Connor TR, Sikes JG, Obradovic Z, and Dunker AK (2004). The importance of intrinsic disorder for protein phosphorylation. *Nucleic Acids Res* 32, 1037–1049. 10.1093/nar/gkh253. [PubMed: 14960716]
85. Bondos SE, Dunker AK, and Uversky VN (2022). Intrinsically disordered proteins play diverse roles in cell signaling. *Cell Commun Signal* 20, 20. 10.1186/s12964-022-00821-7. [PubMed: 35177069]
86. Galea CA, Nourse A, Wang Y, Sivakolundu SG, Heller WT, and Kriwacki RW (2008). Role of intrinsic flexibility in signal transduction mediated by the cell cycle regulator, p27 Kip1. *J Mol Biol* 376, 827–838. 10.1016/j.jmb.2007.12.016. [PubMed: 18177895]
87. Elly C, Witte S, Zhang Z, Rosnet O, Lipkowitz S, Altman A, and Liu YC (1999). Tyrosine phosphorylation and complex formation of Cbl-b upon T cell receptor stimulation. *Oncogene* 18, 1147–1156. 10.1038/sj.onc.1202411. [PubMed: 10022120]
88. Myers DR, Zikherman J, and Roose JP (2017). Tonic Signals: Why Do Lymphocytes Bother? *Trends Immunol* 38, 844–857. 10.1016/j.it.2017.06.010. [PubMed: 28754596]
89. Stefanova I, Dorfman JR, and Germain RN (2002). Self-recognition promotes the foreign antigen sensitivity of naive T lymphocytes. *Nature* 420, 429–434. 10.1038/nature01146. [PubMed: 12459785]
90. Garcia-Morales P, Minami Y, Luong E, Klausner RD, and Samelson LE (1990). Tyrosine phosphorylation in T cells is regulated by phosphatase activity: studies with phenylarsine oxide. *Proc Natl Acad Sci U S A* 87, 9255–9259. 10.1073/pnas.87.23.9255. [PubMed: 1701256]
91. Courtney AH, Shvets AA, Lu W, Griffante G, Mollenauer M, Horkova V, Lo WL, Yu S, Stepanek O, Chakraborty AK, and Weiss A (2019). CD45 functions as a signaling gatekeeper in T cells. *Sci Signal* 12. 10.1126/scisignal.aaw8151.
92. van Oers NS, Killeen N, and Weiss A (1994). ZAP-70 is constitutively associated with tyrosine-phosphorylated TCR zeta in murine thymocytes and lymph node T cells. *Immunity* 1, 675–685. 10.1016/1074-7613(94)90038-8. [PubMed: 7600293]
93. Kamphorst AO, Wieland A, Nasti T, Yang S, Zhang R, Barber DL, Konieczny BT, Daugherty CZ, Koenig L, Yu K, et al. (2017). Rescue of exhausted CD8 T cells by PD-1-targeted therapies is CD28-dependent. *Science* 355, 1423–1427. 10.1126/science.aaf0683. [PubMed: 28280249]
94. Roiniotis J, Dinh H, Masendycz P, Turner A, Elsegood CL, Scholz GM, and Hamilton JA (2009). Hypoxia prolongs monocyte/macrophage survival and enhanced glycolysis is associated with their maturation under aerobic conditions. *J Immunol* 182, 7974–7981. 10.4049/jimmunol.0804216. [PubMed: 19494322]
95. Borregaard N, and Herlin T (1982). Energy metabolism of human neutrophils during phagocytosis. *J Clin Invest* 70, 550–557. 10.1172/jci110647. [PubMed: 7107894]
96. Krawczyk CM, Holowka T, Sun J, Blagih J, Amiel E, DeBerardinis RJ, Cross JR, Jung E, Thompson CB, Jones RG, and Pearce EJ (2010). Toll-like receptor-induced changes in glycolytic metabolism regulate dendritic cell activation. *Blood* 115, 4742–4749. 10.1182/blood-2009-10-249540. [PubMed: 20351312]

97. Frank D, Naseem S, Russo GL, Li C, Parashar K, Konopka JB, and Carpino N (2018). Phagocytes from Mice Lacking the Sts Phosphatases Have an Enhanced Antifungal Response to *Candida albicans*. *MBio* 9. 10.1128/mBio.00782-18.
98. Veeramani S, Lee MS, and Lin MF (2009). Revisiting histidine-dependent acid phosphatases: a distinct group of tyrosine phosphatases. *Trends Biochem Sci* 34, 273–278. 10.1016/j.tibs.2009.03.002. [PubMed: 19467874]
99. Kurachi M, Kurachi J, Chen Z, Johnson J, Khan O, Bengsch B, Stelekati E, Attanasio J, McLane LM, Tomura M, et al. (2017). Optimized retroviral transduction of mouse T cells for in vivo assessment of gene function. *Nat Protoc* 12, 1980–1998. 10.1038/nprot.2017.083. [PubMed: 28858287]
100. Pai CS, Huang JT, Lu X, Simons DM, Park C, Chang A, Tamaki W, Liu E, Roybal KT, Seagal J, et al. (2019). Clonal Deletion of Tumor-Specific T Cells by Interferon-gamma Confers Therapeutic Resistance to Combination Immune Checkpoint Blockade. *Immunity* 50, 477–492 e478. 10.1016/j.immuni.2019.01.006. [PubMed: 30737146]
101. Crooks GE, Hon G, Chandonia JM, and Brenner SE (2004). WebLogo: a sequence logo generator. *Genome Res* 14, 1188–1190. 10.1101/gr.849004. [PubMed: 15173120]

Highlights

- STS1 is inducibly recruited to Cbl-b to dephosphorylate TCR signaling molecules
- The TCR induced STS1/Cbl-b complex restrains T cell responses at acidic pH
- STS1 and Cbl-b restrain T cell responses under intra- or extracellular acidic pH
- *STS1* or *Cbl-b* deletion improves T cell anti-tumor responses and inhibits tumor growth

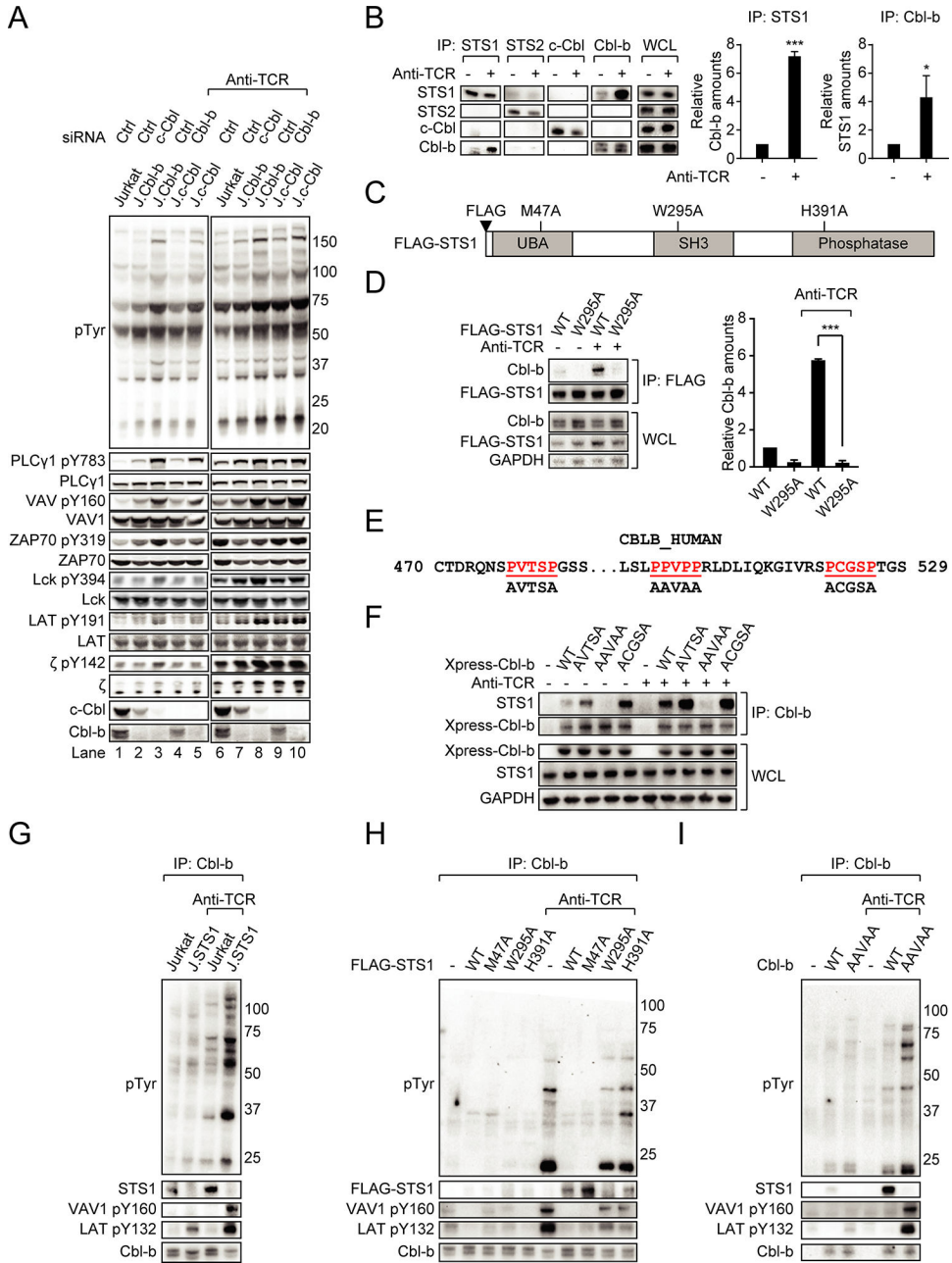


Figure 1. STS1 interacts with Cbl-b PPVPP motif using its SH3 domain to dephosphorylate TCR signaling molecules.

(A) Immunoblot using lysates from WT, *Cbl-b*^{-/-} (*J.Cbl-b*) or *c-Cbl*^{-/-} (*J.c-Cbl*) Jurkat cells transfected with Ctrl or *c-Cbl* and *Cbl-b* targeting siRNA and stimulated with anti-TCR antibodies.

(B) Same as (A) except the whole cell lysates (WCLs) were subjected to immunoprecipitation (IP) using indicated antibodies. The relative Cbl-b and STS1 amounts in the IP fraction were quantified.

(C) Locations of the FLAG-tag and domains of STS1. Defective mutant for each domain is indicated.

- (D) Same as (B) except *STSI*^{-/-} Jurkat (J.STS1) cells transfected with WT or mutant W295A were used for anti-FLAG IP.
- (E) Predicted proline-rich regions (PRRs) on Cbl-b between AA 470 and 529. For the PRR-defective mutants, proline residues in each PRR were replaced by alanine.
- (F) Same as (D) except J.Cbl-b cells reconstituted with WT or PRR mutants were used for anti-Cbl-b IP.
- (G) Same as (B) except Jurkat and J.STS1 cells were used for anti-Cbl-b IP.
- (H) Same as (G) except J.STS1 cells reconstituted with WT and mutants were used.
- (I) Same as (G) except J.Cbl-b cells reconstituted with WT and mutant AAVAA were used.

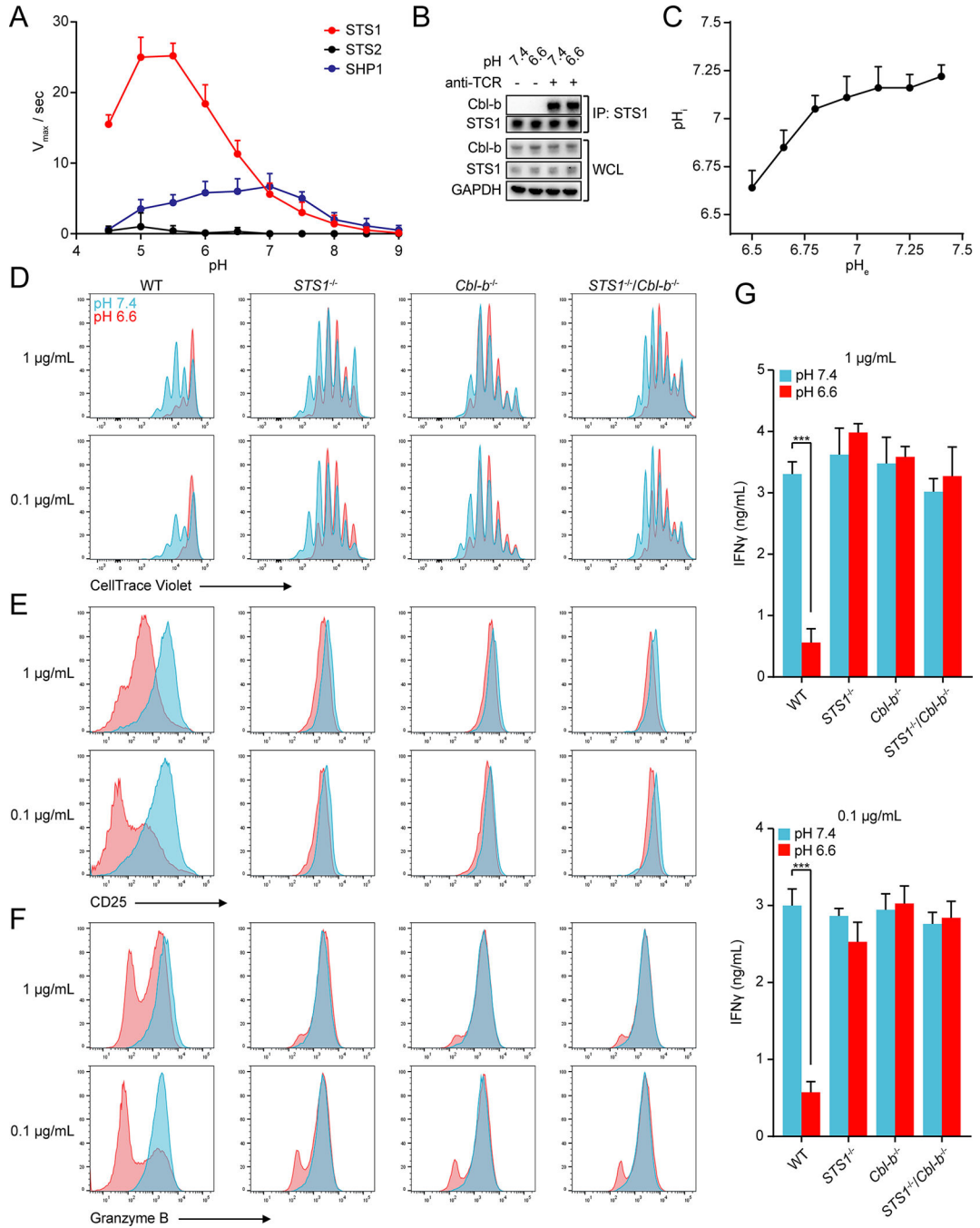


Figure 2. Acidic pH_e -induced suppression of T cell function is mediated by STS1 and Cbl-b.

(A) *In vitro* phosphatase assay using DifMUP as substrate and the phosphatase domains of the indicated recombinant proteins under different pH.

(B) Immunoblot using lysates from Jurkat cells stimulated with anti-TCR antibodies in PBS at indicated pH_e . WCLs were subjected to STS1 IP.

(C) Measured pH_i of T cells in indicated pH_e buffer.

(D) *In vitro* proliferation of CD8⁺ T cells from WT, *STSL*, *Cbl-b* single or doubly deficient mice labeled with CellTrace Violet and stimulated by plate-bound anti-CD3 antibody for 72 hr at 1 or 0.1 μg/mL at pH_e 7.4 or 6.6.

(E) Same as (D) except CD25 was detected.

(F) Same as (D) except granzyme B was detected.

(G) Same as (D) except IFN γ in the medium was detected by ELISA.

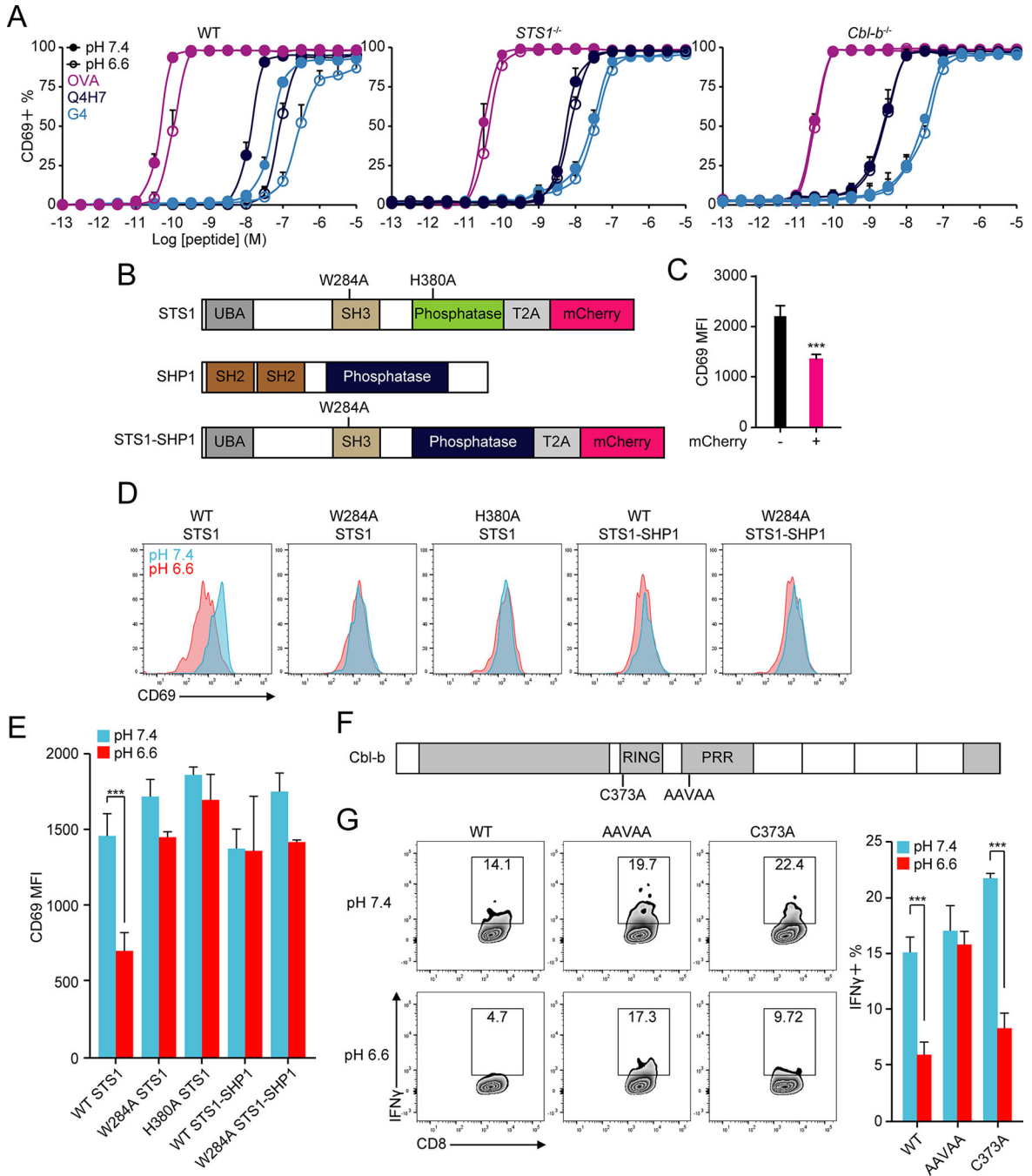


Figure 3. Acidic pH_e induced T cell suppression is mediated by the unconventional phosphatase domain of STS1.

(A) CD69 induction of WT, $STS1^{-/-}$ or $Cbl-b^{-/-}$ OT-1 T cells incubated with splenocytes loaded with different concentrations of OVA, Q4H7 and G4 peptides at pH_e 7.4 or 6.6 overnight.

(B) STS1 mutant constructs. Location of each mutation was shown. STS1-SHP1 chimeric mutant was created by replacing the STS1 phosphatase domain with SHP1 phosphatase domain.

(C) CD69 induction of *STST^{-/-}* OT-1 T cells expressing STS1-SHP1 chimera stimulated with G4 peptide-loaded splenocytes. The CD69 median fluorescence intensities (MFIs) of STS1-SHP1-reconstituted cells (mCherry⁺) and non-reconstituted cells (mCherry⁻) were quantified.

(D) Same as (C) except cells were reconstituted with WT STS1 or different mutants and stimulated at pH_e 7.4 or 6.6.

(E) Quantification of CD69 MFIs from (D).

(F) Cbl-b mutants used to study pH sensitivity. Murine Cbl-b was coupled to T2A-EGFP at the C-terminus for gating purposes (not shown). Location of each mutant is depicted.

(G) IFN γ expression in *Cbl-b^{-/-}* OT-1 T cells expressing Cbl-b mutants stimulated with G4 peptide-loaded splenocytes at pH_e 7.4 or 6.6.

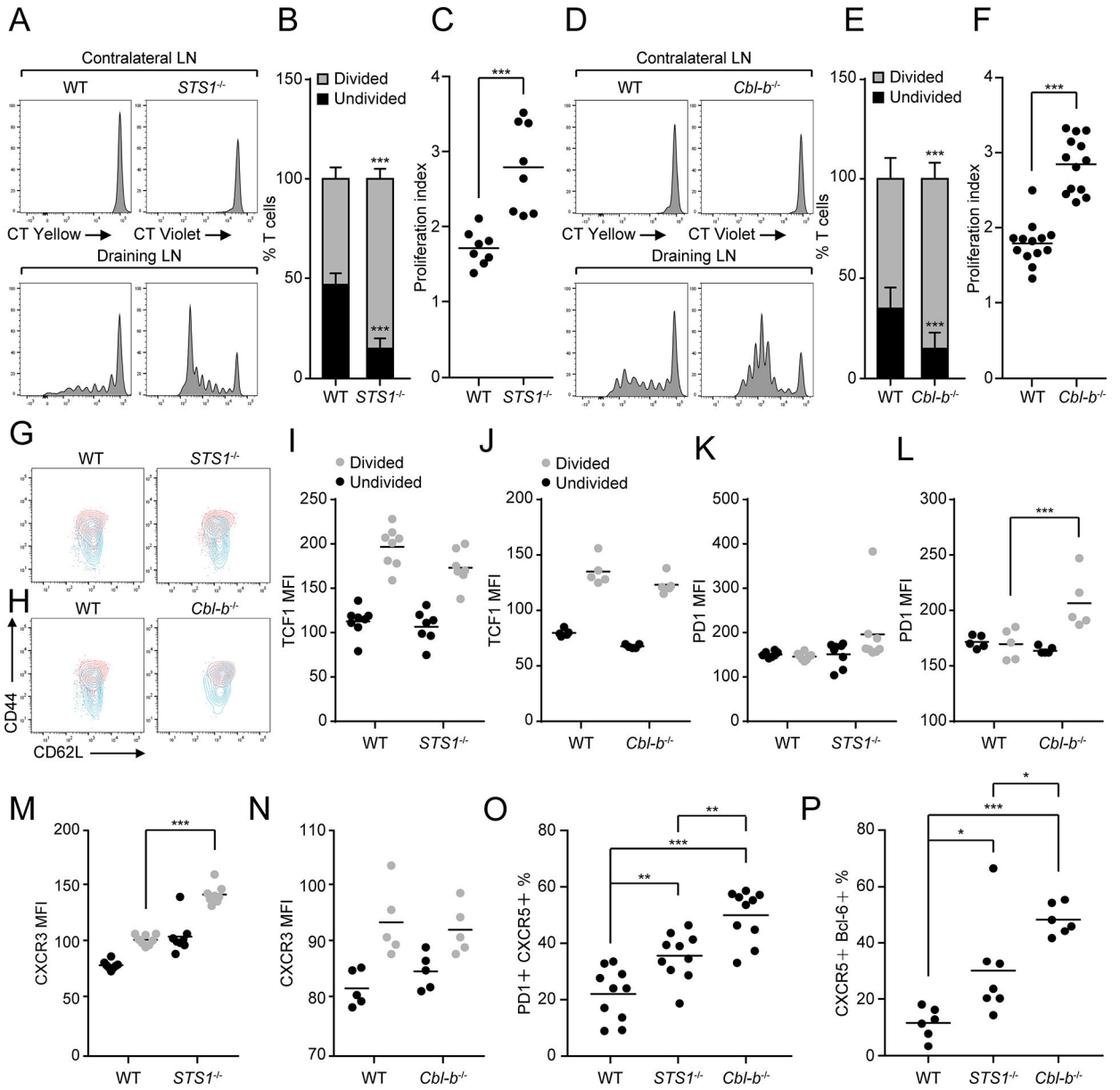


Figure 4. Suppression of T cell proliferation and differentiation *in vivo* is mediated by *STS1* and *Cbl-b*.

(A) *In vivo* proliferation of WT OT-1 T cells (CellTrace Yellow-labeled) and *STS1*^{-/-} OT-1 T cells (CellTrace Violet-labeled) in the lymph nodes (LNs) after ovalbumin stimulation.

(B) Quantification of divided and undivided populations of WT and *STS1*^{-/-} OT-1 cells in (A).

(C) Proliferation index of WT and *STS1*^{-/-} OT-1 T cells in (A).

(D) Same as (A) except WT and *Cbl-b*^{-/-} OT-1 T cells were used.

(E) Same as (B) except WT and *Cbl-b*^{-/-} OT-1 T cells were used.

(F) Proliferation index of WT and *Cbl-b*^{-/-} OT-1 T cells in (D).

(G) Same as (A) except CD44 and CD62L expressions are plotted.

(H) Same as (G) except WT and *Cbl-b*^{-/-} OT-1 T cells were used.

- (I) Same as (G) except TCF1 expression in divided and undivided cells was analyzed. The MFIs of TCF1 were quantified.
- (J) Same as (I) except WT and *Cbl-b*^{-/-} OT-1 T cells were used.
- (K) Same as (I) except PD1 expression was analyzed.
- (L) Same as (K) except WT and *Cbl-b*^{-/-} OT-1 T cells were used.
- (M) Same as (K) except CXCR3 expression was analyzed.
- (N) Same as (M) except WT and *Cbl-b*^{-/-} OT-1 T cells were used.
- (O) *In vivo* Tfh differentiation of WT, *STSL*^{-/-} or *Cbl-b*^{-/-} OT-2 T cells after ovalbumin stimulation. PD1⁺ CXCR5⁺ OT-2 T cells were quantified.
- (P) Same as (O) except CXCR5⁺ Bcl-6⁺ OT-2 T cells were quantified.

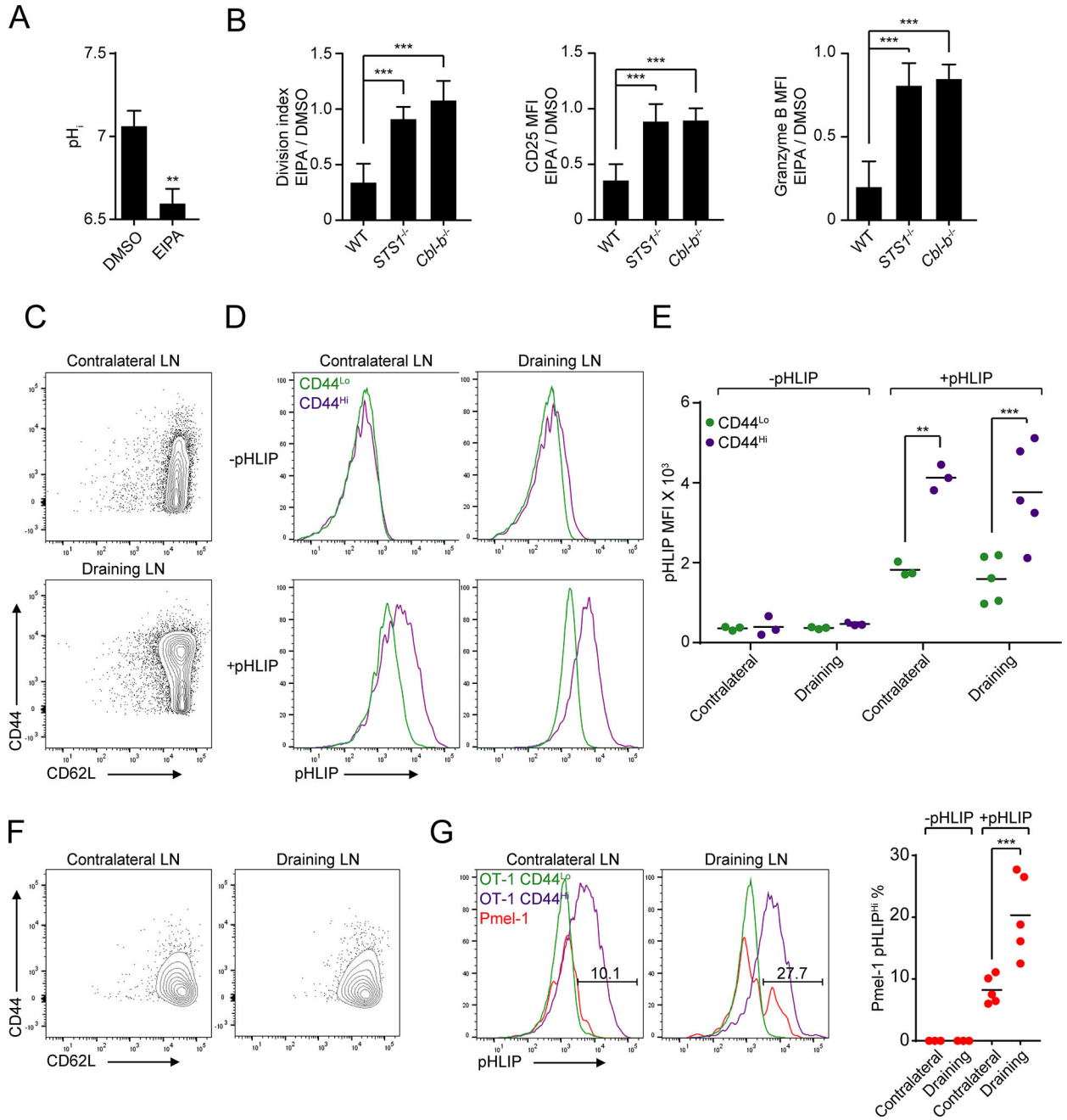


Figure 5. Assessment of autocrine and paracrine acid sources *in vivo*.

(A) Measured pH_i of T cells treated with vehicle or EIPA and stimulated by plate-bound anti-CD3 antibodies for 72 hr.

(B) Same as (A) except cells were assessed for proliferative response or CD25 and Granzyme B expressions.

(C) OT-1 mice were injected with ovalbumin in the footpad for 72 hr, followed by Cy5-pHLIP in the hock.

CD44 and CD62L expression of OT-1 T cells in the popliteal LNs were plotted. (D) Same as (C) except Cy5-pHLIP was detected in CD44^{Hi} and CD44^{Lo} populations.

(E) The MFIs of Cy5-pHLIP in (D) were quantified.

(F) Scheme same as (C) except 10^6 Pmel-1 T cells were adoptively transferred into OT-1 mice before the treatment. CD44 and CD62L expression of Pmel-1 T cells in the LNs were plotted.

(G) Same as (F) except Cy5-pHLIP was detected in CD44^{Hi}, CD44^{Lo} OT-1 and Pmel-1 T cells. The percentages of pHLIP^{Hi} Pmel-1 T cells in the LNs were quantified.

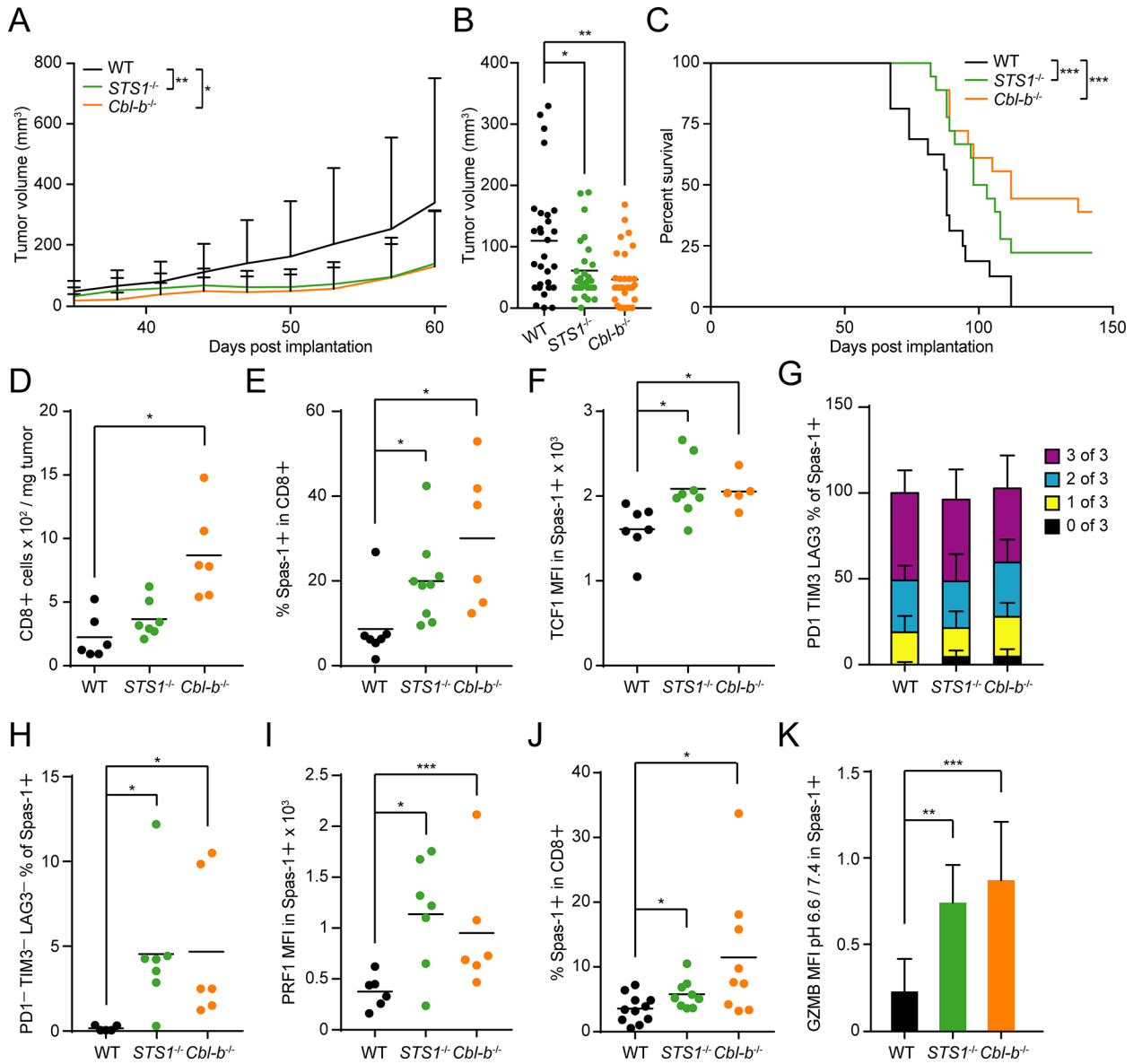


Figure 6. *STS1* or *Cbl-b* deficiencies suppressed prostate tumor progression.

(A) TRAMP-C2 tumor growth at the right flank in WT, *STS1*^{-/-} or *Cbl-b*^{-/-} mice. Tumor sizes were measured twice weekly.

(B) Tumor volumes measured at 45 days post tumor implantation.

(C) Survival of mice implanted with tumor cells.

(D) Number of CD3⁺ CD8⁺ T cells normalized per mg of tumor. Tumor-infiltrating T cells were analyzed by flow cytometry. Gated CD45⁺ CD3⁺ CD8⁺ cells are shown.

(E) Quantification of percentages of Spas-1-specific (Spas-1⁺) CD8⁺ T cells in (D).

(F) Quantification of the MFIs of TCF1 in Spas-1⁺ T cells in (E).

(G) Same as (F) except PD1, TIM3 and LAG3 were detected. Quantification of percentages of T cells positive for 0, 1, 2, or 3 proteins.

(H) Quantification of PD1⁻ TIM3⁻ LAG3⁻ populations in (G).

(I) Quantification of PRF1 MFIs in Spas-1⁺ T cells in (E).

(J) Same as (D) except spleocytes were used. The percentages of Spas-1⁺ CD8⁺ T cells were quantified.

(K) Splenocytes from tumor-bearing mice were stimulated with anti-CD3/CD28 antibody-coated beads at pH_e 7.4 or 6.6. After 72 hr, Granzyme B in Spas-1-specific CD8⁺ T cells were analyzed. The ratios of granzyme B MFI of cells cultured in pH_e 6.6 to 7.4 were quantified.

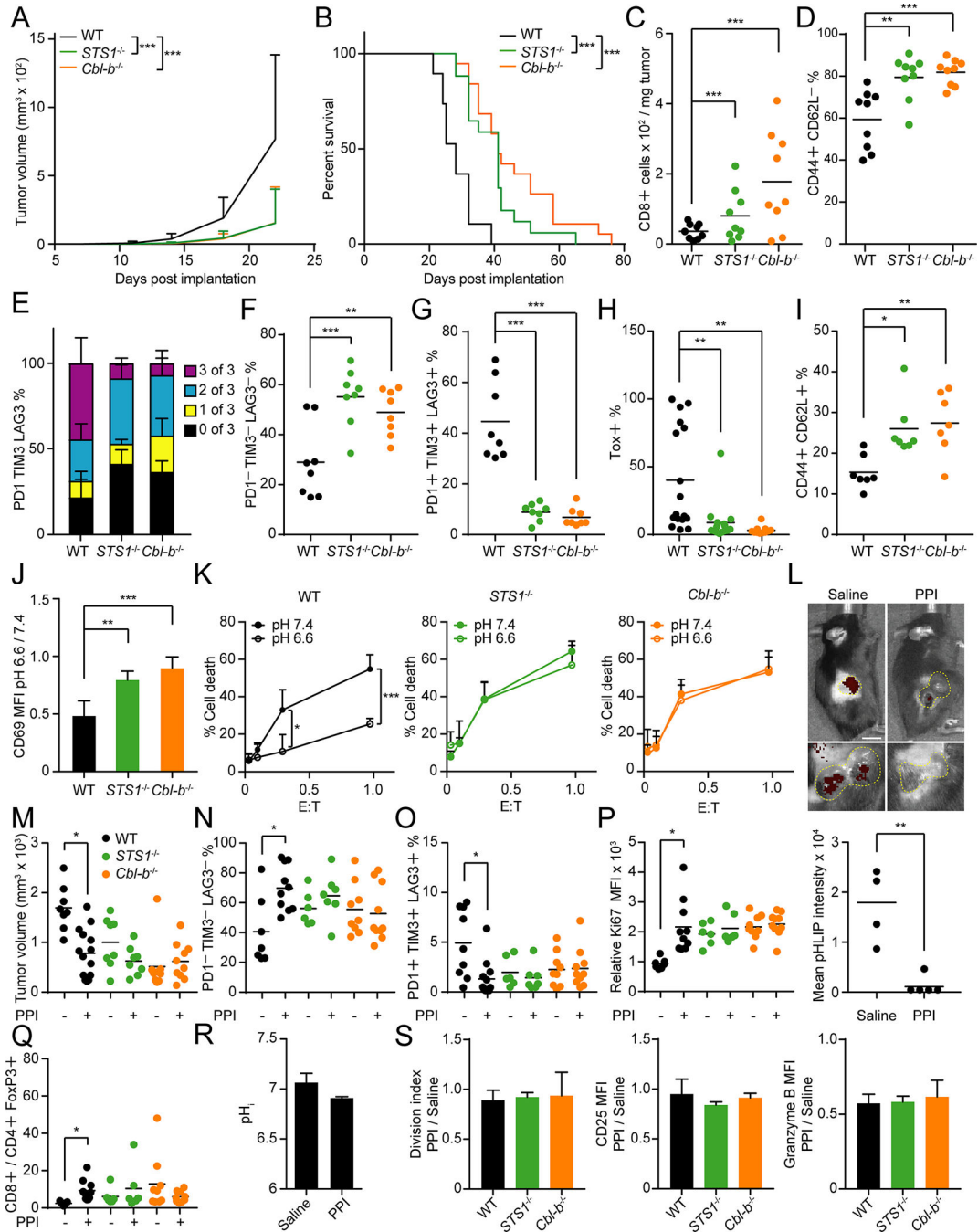


Figure 7. Neutralizing the acidic TME pH_e improvement of T cell function depended on *STS1* or *Cbl-b*.

(A) B16-F10 melanoma growth in the right flank of WT, *STS1*^{-/-} or *Cbl-b*^{-/-} Pmel-1 mice.

Tumor sizes were measured twice weekly.

(B) Survival of mice implanted with tumor cells.

(C) Number of CD8⁺ Vβ13⁺ Pmel-1 T cells normalized to mg of tumor. Tumor-infiltrating T cells were analyzed by flow cytometry. Gated CD8⁺ Vβ13⁺ cells are shown.

(D) Quantification of CD44⁺ CD62L⁻ population in (C).

- (E) PD1, TIM3 and LAG3 were detected within CD8⁺ Vβ13⁺ T cells. Quantification of percentages of T cell positive for 0, 1, 2, or 3 proteins.
- (F) Quantification of PD1⁻ TIM3⁻ LAG3⁻ populations in (E).
- (G) Quantification of PD1⁺ TIM3⁺ LAG3⁺ populations in (E).
- (H) Quantification of Tox⁺ population in (C).
- (I) Same as (C) except splenocytes were used. The percentages of CD44⁺ CD62L⁺ population in Vβ13⁺ CD8⁺ T cells were quantified.
- (J) Splenocytes from tumor-bearing mice were stimulated with mgp100 peptide in pH_e 7.4 or 6.6 overnight. The MFIs of CD69 on CD8⁺ Vβ13⁺ T cells were quantified. The ratios of CD69 MFI in pH_e 6.6 to 7.4 were quantified.
- (K) WT, *STSI*^{-/-} and *Cbl-b*^{-/-} OT-1 T cells were stimulated with OVA peptide-loaded splenocytes in pH_e 7.4 or 6.6, followed by fresh medium with IL-2. Cytolytic T cells were co-cultured with ovalbumin-expressing B16-F10 cells at different effector-to-target (E:T) cell ratios for 72 hr. The percentages of dead cancer cells were detected by flow cytometry and quantified.
- (L) Mice were injected with saline or esomeprazole (PPI) 24 hr before Cy5-pHLIP injection. Tumor areas were circled in yellow and the MFIs were quantified by ImageJ. Scale bar = 13 mm.
- (M) Same as (A) except one day after tumor size reached 100 mm³, mice were injected with PPI every other day for total 6 injections. Tumor volumes were measured at the day of harvest.
- (N) Quantification of PD1⁻ TIM3⁻ LAG3⁻ populations in CD8⁺ Vβ13⁺ tumor-infiltrating T cells in (M).
- (O) Same as (N) except the percentages of PD1⁺ TIM3⁺ LAG3⁺ populations were quantified.
- (P) Same as (N) except the MFIs of Ki67 were quantified.
- (Q) Same as (N) except the ratios of CD8⁺/T_{reg} were quantified.
- (R) Measured pH_i of T cells treated with PPI and stimulated by plate-bound anti-CD3 antibodies for 72 hr.
- (S) Same as (R) except cells were subjected to the detection of proliferation, CD25 and Granzyme B expressions.

REAGENT or RESOURCE	SOURCE	IDENTIFIER
Antibodies		
Mouse monoclonal anti-Bcl-6	BD Biosciences	AB_10898007
Rabbit monoclonal anti-Cbl-b	Cell Signaling Technology	AB_2797707
Rabbit polyclonal anti-Cbl-b	Proteintech	AB_2275326
Rabbit polyclonal anti-c-Cbl	Cell Signaling Technology	AB_2275284
Rat monoclonal anti-CD16/CD32	Tonbo Biosciences	AB_2621487
Mouse monoclonal anti-CD25	BD Biosciences	AB_394604
Mouse monoclonal anti-CD25	BD Biosciences	AB_2738304
Hamster monoclonal anti-CD3e	Weiss lab	N/A
Hamster monoclonal anti-CD3e	BD Biosciences	AB_2738278
Hamster monoclonal anti-CD3e	BD Biosciences	AB_2870231
Hamster monoclonal anti-CD3e	BioLegend	AB_312671
Hamster monoclonal anti-CD3e	BioLegend	AB_312673
Rat monoclonal anti-CD4	BD Biosciences	AB_2738426
Rat monoclonal anti-CD4	BioLegend	AB_2564586
Rat monoclonal anti-CD44	BD Biosciences	AB_2739963
Rat monoclonal anti-CD44	BioLegend	AB_2562600
Rat monoclonal anti-CD44	BD Biosciences	AB_10895375
Rat monoclonal anti-CD44	BD Biosciences	AB_10894581
Mouse monoclonal anti-CD45	BioLegend	AB_493535
Mouse monoclonal anti-CD45.1	BD Biosciences	AB_2861197
Mouse monoclonal anti-CD45.2	BD Biosciences	AB_395041
Mouse monoclonal anti-CD45.2	Tonbo Biosciences	AB_2621950
Rat monoclonal anti-CD45R	BD Biosciences	AB_394618
Rat monoclonal anti-CD45R	Tonbo Biosciences	AB_2621948
Rat monoclonal anti-CD62L	BioLegend	AB_10900082
Rat monoclonal anti-CD62L	BioLegend	AB_10900262
Rat monoclonal anti-CD62L	BD Biosciences	AB_2740349
Hamster monoclonal anti-CD69	BD Biosciences	AB_10893008
Hamster monoclonal anti-CD69	BD Biosciences	AB_2739968
Hamster monoclonal anti-CD69	BD Biosciences	AB_394726
Hamster monoclonal anti-CD69	BioLegend	AB_940497
Mouse monoclonal anti-CD69	BD Biosciences	AB_400353
Mouse monoclonal anti-CD69	BD Biosciences	AB_400523
Rat monoclonal anti-CD73	BD Biosciences	AB_10714078
Rat monoclonal anti-CD8	BioLegend	AB_2563237
Rat monoclonal anti-CD8	BioLegend	AB_389326
Rat monoclonal anti-CD8	BioLegend	AB_312745

REAGENT or RESOURCE	SOURCE	IDENTIFIER
Rat monoclonal anti-CD8	BD Biosciences	AB_2732919
Rat monoclonal anti-CD8	BD Biosciences	AB_2870186
Rat monoclonal anti-CD8	BD Biosciences	AB_394571
hamster monoclonal anti-CXCR3	BioLegend	AB_2563160
Rat monoclonal anti-CXCR5	BD Biosciences	AB_1727520
Rat monoclonal anti-EGFP	BioLegend	AB_2563287
Rabbit monoclonal anti-Erk1/2	Cell Signaling Technology	AB_331775
Mouse monoclonal anti-FLAG-tag	MilliporeSigma	AB_262044
Rat monoclonal anti-FoxP3	Thermo Fisher Scientific	AB_465243
Rat monoclonal anti-FoxP3	Thermo Fisher Scientific	AB_891554
Rat monoclonal anti-FR4	BD Biosciences	AB_1645227
Rabbit monoclonal anti-GAPDH	Cell Signaling Technology	AB_561053
Mouse monoclonal anti-Granzyme B	BioLegend	AB_2294995
Mouse monoclonal anti-Granzyme B	BioLegend	AB_2114575
Mouse monoclonal anti-Granzyme B	BioLegend	AB_2562196
Mouse monoclonal anti-GST	MilliporeSigma	AB_309675
Rat monoclonal anti-IFN γ	BD Biosciences	AB_2738752
Mouse monoclonal anti-Ki67	BD Biosciences	AB_10611866
Rat monoclonal anti-LAG3	BioLegend	AB_2133343
Rat monoclonal anti-LAG3	BioLegend	AB_2566571
Rabbit polyclonal anti-LAT	Cell Signaling Technology	AB_2283298
Rabbit polyclonal anti-LAT pY132	Abcam	AB_304482
Rabbit polyclonal anti-LAT pY191	Cell Signaling Technology	AB_2157728
Rabbit monoclonal anti-Lck pY394	Cell Signaling Technology	AB_10013641
Rat monoclonal anti-PD1	BioLegend	AB_2159183
Rat monoclonal anti-PD1	BioLegend	AB_2561447
Rat monoclonal anti-PD1	BD Biosciences	AB_2873680
Rat monoclonal anti-PD1	BioLegend	AB_1877087
Rat monoclonal anti-PD1	BioLegend	AB_2566547
Mouse monoclonal anti-PLC γ 1	BD Biosciences	AB_397446
Rabbit polyclonal anti-PLC γ 1 pY783	Thermo Fisher Scientific	AB_1501937
Mouse monoclonal anti-phospho-Tyr	MilliporeSigma	AB_916371
Rat monoclonal anti-PRF1	BioLegend	AB_2721462
Mouse monoclonal anti-SLP76 pY128	BD Biosciences	AB_647331
Rabbit polyclonal anti-SLP76 pY145	Cell Signaling Technology	AB_2798604
Rabbit polyclonal anti-STS1	Abcam	AB_778147
Rabbit polyclonal anti-STS2	Proteintech	AB_2272584
Rat monoclonal anti-TIM3	BioLegend	AB_1626175
Rat monoclonal anti-TIM3	BioLegend	AB_2632736

REAGENT or RESOURCE	SOURCE	IDENTIFIER
Mouse monoclonal anti-TCF1	BD Biosciences	AB_2869823
Mouse monoclonal anti-TCR	Weiss lab	N/A
Rat monoclonal anti-TCR V α 2	BD Biosciences	AB_2741793
Rat monoclonal anti-TCR V α 2	BioLegend	AB_1134183
Rat monoclonal anti-TCR V α 2	BioLegend	AB_2814020
Mouse monoclonal anti-TCR V β 13	BD Biosciences	AB_394706
Mouse monoclonal anti-TCR V β 13	BD Biosciences	AB_10898187
Mouse monoclonal anti-TCR V β 13	BD Biosciences	AB_10924602
Rat monoclonal anti-TOX	Thermo Fisher Scientific	AB_10855034
Rabbit polyclonal anti-VAV1	Santa Cruz Biotechnology	AB_632586
Mouse monoclonal anti-VAV1 pY160	R&D Systems	AB_11127214
Mouse monoclonal anti-Xpress-tag	Thermo Fisher Scientific	AB_2556552
Rabbit monoclonal anti-ZAP70	Cell Signaling Technology	AB_2218656
Rabbit polyclonal anti-ZAP70 pY319	Cell Signaling Technology	AB_331600
Rabbit polyclonal anti-ZAP70 pY493	Cell Signaling Technology	AB_2217457
Mouse monoclonal anti- ζ	BD Biosciences	AB_394011
Mouse monoclonal anti- ζ pY142	BD Biosciences	AB_647307
Bacterial and virus strains		
<i>Escherichia coli</i> 5-alpha	New England Biolabs	Cat#C2987H
Chemicals, peptides, and recombinant proteins		
3-MB-PP1	Cayman Chemical	Cat#17860
BCECF	Thermo Fisher Scientific	Cat#B1170
Bovine insulin	MilliporeSigma	Cat#I0516
Collagenase IV	MilliporeSigma	Cat#C5138
DAPI	Thermo Fisher Scientific	Cat#D3571
Dehydroisoandrosterone	MilliporeSigma	Cat#D5297
DifMUP	Thermo Fisher Scientific	Cat#D6567
DNase I	MilliporeSigma	Cat#D4263
EIPA	Barber Laboratory	N/A
Esomeprazole	MilliporeSigma	Cat#E7906
G4	GenScript	Customized synthesis
Glutathione	MilliporeSigma	Cat#G4251
Golgiplug	BD Biosciences	Cat#555029
Mgp100 ₂₅₋₃₃	GenScript	Customized synthesis
OVA	GenScript	Customized synthesis
pH Low insertion peptide	GenScript	Customized synthesis
PP2	MilliporeSigma	Cat#P0042

REAGENT or RESOURCE	SOURCE	IDENTIFIER
Puromycin	MilliporeSigma	Cat#P8833
Q4H7	GenScript	Customized synthesis
Q4R7	GenScript	Customized synthesis
Recombinant GST-ST51 SH3 domain	This study	N/A
Recombinant human IL-2	R&D Systems	Cat#202-IL-500
Recombinant SHP1 phosphatase domain	R&D systems	Cat#1878-SH
Recombinant STS1 phosphatase domain	Sino Biological	Cat#13868-H07E
Recombinant STS2 phosphatase domain	Sino Biological	Cat#13847-H07E
SPAS-1 tetramer	NIH Tetramer core	N/A
Streptavidin	Jackson ImmunoResearch	Cat#016-000-113
T4	GenScript	Customized synthesis
Turbofect	Thermo Fisher Scientific	Cat#R0531
VSV	GenScript	Customized synthesis
Critical commercial assays		
BD Cytotfix™ Fixation Buffer	BD Biosciences	Cat#554655
BD OptEIA™ Mouse IL-2 ELISA Set	BD Biosciences	Cat#555148
BD OptEIA™ Mouse IFN- γ ELISA Set	BD Biosciences	Cat#555138
Foxp3 / Transcription Factor Staining Buffer Set	Thermo Fisher Scientific	Cat#00-5523-00
Intracellular pH Calibration Buffer Kit	Thermo Fisher Scientific	Cat#P35379
Experimental models: Cell lines		
Human: 293	UCSF Cell and Genome Engineering Core	N/A
Human: 293T	UCSF Cell and Genome Engineering Core	N/A
Human: J.Cbl-b	This study	N/A
Human: J.Cbl-b.3YF	This study	N/A
Human: J.Cbl-b.AAVAA	This study	N/A
Human: J.Cbl-b.ACGSA	This study	N/A
Human: J.Cbl-b.AVTSA	This study	N/A
Human: J.Cbl-b.C373A	This study	N/A
Human: J.Cbl-b.G298E	This study	N/A
Human: J.Cbl-b.M940A	This study	N/A
Human: J.Cbl-b.STS1	This study	Clone 34
Human: J.Cbl-b.STS1	This study	Clone 37

REAGENT or RESOURCE	SOURCE	IDENTIFIER
Human: J.Cbl-b.STS1	This study	Clone 40
Human: J.Cbl-b.WT	This study	N/A
Human: J.Cbl-b.Y363F	This study	N/A
Human: J.Cbl-b.Y665F	This study	N/A
Human: J.Cbl-b.Y665F Y709F	This study	N/A
Human: J.Cbl-b.Y665F Y889F	This study	N/A
Human: J.Cbl-b.Y709F	This study	N/A
Human: J.Cbl-b.Y709F Y889F	This study	N/A
Human: J.Cbl-b.Y889F	This study	N/A
Human: J.c-Cbl	This study	N/A
Human: J.STS1	This study	Clone 8
Human: J.STS1	This study	Clone 9
Human: J.STS1	This study	Clone 13
Human: J.STS1 H391A	This study	N/A
Human: J.STS1 M47A	This study	N/A
Human: J.STS1 W295A	This study	N/A
Human: J.STS1 WT	This study	N/A
Human: J.ZAP	Weiss Laboratory	Clone 2
Human: Jurkat	Weiss Laboratory	N/A
Human: P116.ZAP70 ^{AS}	Weiss Laboratory	Clone 2
Human: Phoenix-Eco	UCSF Cell and Genome Engineering Core	N/A
Mouse: B16-F10	ATCC	Cat#CRL-6475
Mouse: Ovalbumin-expressing B16-F10	Krummel Laboratory	N/A
Mouse: TRAMP-C2	ATCC	Cat#CRL-2731
Experimental models: Organisms/strains		
B6.129S2- <i>Tcrat^{m1Mom}/J</i>	The Jackson Laboratory	Cat#002116
B6.Cg-Tg(<i>Tcratcrb</i>)425Cbn/J	The Jackson Laboratory	Cat#004194
B6.Cg- <i>Thy1^l/Cy</i> Tg(<i>Tcratcrb</i>)8Rest/J	The Jackson Laboratory	Cat#005023
B6.SJL- <i>Ptprca²Pepc^b/BoyJ</i>	The Jackson Laboratory	Cat#002014
C57BL/6J mice	The Jackson Laboratory	Cat#000664
C57BL/6-Tg(<i>Tcratcrb</i>)1100Mjb/J	The Jackson Laboratory	Cat#003831
Cbl-b ^{-/-} mice	Gu Laboratory	N/A
STS1 ^{-/-} Cbl-b ^{-/-} mice	Weiss Laboratory	N/A
STS1 ^{-/-} mice	Carpino Laboratory	N/A
Oligonucleotides		
Cbl-b-targeting siRNA	Thermo Fisher Scientific	s2479

REAGENT or RESOURCE	SOURCE	IDENTIFIER
c-Cbl-targeting siRNA	Thermo Fisher Scientific	s2477
Cbl-b sgRNA-guiding sequence, forward: CACCGAGCAAGCTGCCGCAGATCGC	Integrated DNA Technologies	Customized synthesis
Cbl-b sgRNA-guiding sequence, reverse: AAACGCGATCTGCGGCAGCTTGCTC	Integrated DNA Technologies	Customized synthesis
c-Cbl sgRNA-guiding sequence, forward: CACCGTGGCCTGATTGGGCTCATGA	Integrated DNA Technologies	Customized synthesis
c-Cbl sgRNA-guiding sequence, reverse: AAACTCATGAGCCCAATCAGGCAC	Integrated DNA Technologies	Customized synthesis
STS1 sgRNA-guiding sequence, forward: CACCGGCTCGGCATGGCTGCCGAGAG	Integrated DNA Technologies	Customized synthesis
STS1 sgRNA-guiding sequence, reverse: AAACCTCTCGCAGCCATGCCGAGCC	Integrated DNA Technologies	Customized synthesis
Recombinant DNA		
pCDEF3	Weiss Laboratory	N/A
pCMV dR8.91	Weiss Laboratory	N/A
pGEX 4T3	Weiss Laboratory	N/A
pHR	Weiss Laboratory	N/A
pMD2.G	Weiss Laboratory	N/A
pX330	Weiss Laboratory	N/A
Software and algorithms		
FlowJo	FlowJo	https://www.flowjo.com
Image Lab	Bio-Rad	http://www.bio-rad.com
ImageJ	NIH	https://imagej.nih.gov/ij/
Living Image	Xenogen	https://spectralin vivo.com/
Prism	GraphPad	http://www.graphpad.com